Journal of Structural Geology 31 (2009) 1377–1394

Contents lists available at ScienceDirect

Journal of Structural Geology

journal homepage: www.elsevier.com/locate/jsg

Constraining deformation stages in brittle–ductile shear zones from combined field mapping and $^{40}Ar/^{39}Ar$ dating: The structural evolution of the Grimsel Pass area (Aar Massif, Swiss Alps)

Yann Rolland [a,*], Stephen F. Cox [b], Michel Corsini [a]

[a] Géosciences Azur, Université de Nice Sophia Antipolis, CNRS, IRD, 28 Av. de Valrose, BP 2135, 06103 Nice, France
[b] Research School of Earth Sciences, The Australian National University, Canberra, ACT 0200, Australia

ARTICLE INFO

Article history:
Received 12 December 2008
Received in revised form
13 July 2009
Accepted 4 August 2009
Available online 11 August 2009

Keywords:
$^{40}Ar/^{39}Ar$ dating
Shear zones
External Crystalline Massifs
Exhumation
Fluid–rock interaction

ABSTRACT

$^{40}Ar/^{39}Ar$ dating of syn-kinematic white mica (phengite) and biotite is used to constrain the age of shear zones within the granodiorites of the Grimsel Pass area (Aar Massif, Central Alps). Three sets of steeply dipping shear zones have been mapped. Stage 1 shear zones are very broad (~200 m wide) zones of biotite-bearing rocks, with a progressive increase in intensity of ductile deformation from rim to core, and have dip-slip kinematics. Subsequent Stage 2 shear zones are narrower, contain phengite-rich mylonites, and show a gradual change from dextral strike-slip to dip-slip kinematics across strike. Strain localisation during the formation of Stage 2 shear zones is interpreted to have been aided by reaction-weakening during extensive fluid–rock interaction. Brittle precursors of Stage 2 shear zones are marked by biotite-rich cataclasites preserved along the northern contact of the overprinting main Stage 2 shear zone.

Biotite from a Stage 1 shear zone yields an age of 21.1 ± 0.2 Ma. Phengites in Stage 2 mylonites in the Grimsel Pass area have a very narrow age range (13.8–12.2 Ma), which is interpreted to bracket the duration of ductile deformation during Stage 2 deformation at mid-crustal levels. However, the biotite-rich cataclasites at the margin of a Stage 2 shear zone may have localised fluid flow up to ~2 Ma prior to the onset of main Stage 2 ductile deformation. Stage 3 shear zones are brittle strike-slip faults containing cataclasites, breccias and clay fault gouges. Earlier studies have established that these late faults formed at <9 Ma and were active until at least 3 Ma.

1. Introduction

Constraining the absolute age and duration of deformation in shear zones is a challenging objective. However, such constraints are critical for establishing P-T-t paths and regional correlations of tectonic phases in orogens, and for understanding the roles of fluid–rock interaction and fluid redistribution processes in general. Major questions that often need to be resolved are: (1) What is the relative age and duration of the commonly observed brittle and ductile components of deformation in middle-crustal shear zones? (2) What is the duration of fluid flow in shear zones? (3) Is it possible to establish the timing of shearing events within a multiply deformed tectonic zone using available dating techniques?

Direct dating of deformation is only feasible for syn-kinematic minerals whose growth can be directly linked to the structural evolution (e.g. Müller et al., 2000a), and whose isotopic clock has not been modified since the time of crystallisation. In low-grade metamorphic environments such as the Alpine External Massifs mineral (re-)crystallisation, is generally partial and restricted to shear zones, which localise deformation and fluid–rock interaction (e.g. Kerrich, 1986; Cox et al., 1987; O'Hara, 1988; McCaig et al., 1990). Syn-kinematic minerals in mylonites are typically fine-grained (<100 μm) and commonly consist of intergrown aggregates of relict host-rock minerals and neo- or re-crystallised metamorphic minerals. As a result, application of classic Rb–Sr and K–Ar techniques remains controversial (Sherlock et al., 2003), although microsampling under direct microscopic control is a promising recent development (Müller et al., 2000a,b). In comparison, the $^{40}Ar/^{39}Ar$ dating method has certain advantages and has been used more frequently for dating low-grade syn-kinematic shear zone minerals (Kligfield et al., 1986; Wijbrans and McDougall, 1986; Kelley, 1988; Goodwin and Renne, 1991; West and Lux, 1993; Kelley et al., 1994; Kirschner et al., 1996; Reddy et al., 1996; Challandes et al., 2003). In particular, laser and oven

* Corresponding author.
E-mail address: yrolland@unice.fr (Y. Rolland).

0191-8141/$ – see front matter © 2009 Elsevier Ltd. All rights reserved.
doi:10.1016/j.jsg.2009.08.003

step-wise heating $^{40}Ar/^{39}Ar$ techniques may allow core-rim alteration and the presence of several mineral generations to be discriminated on the basis of changes in composition and age in different steps of Ar release. However, the meaning of such $^{40}Ar/^{39}Ar$ ages obtained from low temperature shear zone minerals is still a matter of debate. Analytical (Kramar et al., 2001; Mulch et al., 2002) and experimental (Dunlap, 1997; Dunlap and Kronenberg, 2001) studies analysing the effects of deformation on the Ar isotopic system have shown that strain may produce partial Ar loss in pre-existing minerals. Ar loss due to diffusion depends on the mineral size and structure, as well as on the type of deformation (Hames and Bowring, 1994).

Finally, it is generally accepted that direct dating of deformation is possible if dynamic (re-) crystallisation occurred at or below the so-called "closure temperature" of a given mineral (e.g. Dodson, 1973; West and Lux, 1993), although this concept has been challenged by Villa et al. (1997) and Villa (1998). However, in many cases, direct $^{40}Ar/^{39}Ar$ dating of low-grade syn-kinematic minerals does not produce clear and unequivocal results (see review in Rolland et al., 2008). As discussed above, this may be due to (1) partial isotopic resetting during dynamic recrystallisation, (2) mixing between inherited and neo-crystallised minerals, (3) partial Ar loss during ongoing deformation and exhumation, and (4) possible excess ^{40}Ar in shear zones due to strong and possibly heterogeneous fluid–rock interaction.

In the Alpine orogen the relative timing of deformation episodes is generally well established (e.g. Ayrton and Ramsay, 1974; Milnes, 1974; Huber et al., 1980; Burkhard, 1988). Thermo-geochronology has also been extensively employed to constrain the exhumation-time history of the mountain belt (e.g. Wagner et al., 1977; Michalski and Soom, 1990). However, there is still a scarcity of geochronological studies of shear zones that have been closely integrated with an understanding of their structural, microstructural and kinematic evolution. Such deformation ages are necessary to provide absolute constraints on the timing of displacement and deformation within orogens.

Here, we present integrated structural, microstructural and geochronological constraints on the structural evolution of the Grimsel Pass area of the Aar Massif, Central Alps (Fig. 1). In this area, shear zones are well-exposed in glacially polished outcrops. Mapping undertaken in previous works (e.g. Choukroune and Gapais, 1983; Marquer and Gapais, 1985; Marquer et al., 1985; Steck et al., 1999) has demonstrated the presence of anastomosing shear zones, which are thought to have formed during progressive deformation at 22–17 Ma (Challandes et al., 2008). Younger Rb–Sr ages of ~12–10 Ma obtained in the same shear zones were interpreted to be a result late fluid circulation, which post-dated the main deformation event. In the following we show that detailed mapping near the Grimsel Pass, at the southern margin of the Aar Massif, allows recognition of several distinct stages of shear zone evolution, each with different orientation, kinematics and duration. $^{40}Ar/^{39}Ar$ geochronology of syn-kinematic mica was undertaken to constrain the late Alpine structural evolution of the shear zone networks in the Aar Massif. The results presented here complement earlier results by Michalski and Soom (1990), Kralik et al. (1992), Challandes (2001) and Challandes et al. (2008), providing structural and Ar–Ar data showing the superposition of several stages of deformation as an additional basis for reconstruction of the deformation history during exhumation of this part of the Central Alps.

2. Geological context

The Aar Massif is part of the External Crystalline Massifs of the Swiss Alps (Fig. 1) and its geology, structure and metamorphism have been extensively studied over many decades (e.g. Steck, 1966, 1968, 1976, 1984; Steck and Burri, 1971; Frey et al., 1980; Choukroune and Gapais, 1983; von Raumer, 1984; Marquer and Gapais, 1985; Fourcade et al., 1989; Steck et al., 1989; Marquer and Burkhard, 1992; Marquer and Peucat, 1994; Schaltegger, 1994; Frey and Mählmann Ferreiro, 1999; von Raumer et al., 1999). It is composed mainly of two large plutons, the Grimsel granodiorite and the Aar granite both of Late Variscan age, and intruded into Palaeozoic migmatites and amphibolites (Labhart, 1977; Albrecht, 1994; Schaltegger, 1994). These plutons were deformed under greenschist facies conditions during NW-vergent thrusting (Steck, 1966, 1968; Choukroune and Gapais, 1983; Marquer et al., 1985; Marquer, 1987) developed due to Alpine continent–continent collision (e.g. Pfiffner et al., 1990). Alpine deformation within the Massif is heterogeneous, producing anastomosing shear zones (usually with a mylonitic fabric developed toward their centre) that are irregularly distributed within the less deformed host granitoid (Choukroune and Gapais, 1983; Marquer, 1989). Shear zones with subvertical shear planes and down-dip stretching lineations were interpreted to have formed during bulk coaxial NW–SE shortening (Choukroune and Gapais, 1983). The study area, at the southern edge of the Aar Massif, lies in a metamorphic domain located between the stilpnomelane-out and chloritoid-in isograds (Frey, 1987, 1988; Fig. 1). Thermobarometric estimates from mineral assemblages in the shear zones range from 0.3 GPa/400 °C in the north of the massif to 0.6 ± 0.1 GPa/475 ± 25 °C in the study area (Steck and Burri, 1971; Steck, 1976; Bertnoat and Bambauer, 1982; Frey, 1987, 1988; Frey et al., 1980, 1999; Frey and Mählmann Ferreiro, 1999; Challandes et al., 2008). Previous studies have concluded that the shear zones formed at close to peak metamorphic conditions (Fourcade et al., 1989; Challandes, 2001; Challandes et al., 2008). Fluid circulation in the shear zone network is indicated by $\delta^{18}O$ in shear zones being up to 2‰ higher in shear zones than in undeformed zones (Fourcade et al., 1989). Fluid–rock interaction during shear zone formation has also led to enrichment in K, Mg, and Rb and depletion in Na, Ca and Sr within the shear zones compared to the protolith (Marquer et al., 1985; Marquer and Peucat, 1994). This is consistent with the stability of micas and destabilisation of plagioclase during deformation.

As is also the case for the other External Crystalline Massifs (Fig. 1A), the timing of shear zone formation in the Aar Massif is still unclear. One of the main questions addressed in this paper is whether the absolute age discrepancy results either from different exhumation rates if the ages are interpreted as 'closure temperature ages' or they may reflect multi-stage deformation if they represent true 'crystallisation ages'. In the first case, the younger ages obtained in the northern External Crystalline Massifs might be related to the slight increase in maximum temperature reached during the Alpine cycle from south to north (280 °C – 4 kbar in the Pelvoux, to 400–450 °C – 4/5 kbar in the Mont Blanc and Aar Massifs; Simon-Labric et al., 2009; Marquer et al., 1985). But the temperature conditions remain globally below closure temperature of phengite ($T < 450$ °C, Villa et al., 1997). Thus, the ages should have retained the time of crystallisation during deformation. Some previous studies have shown the partial or complete preservation of pre-Alpine K–Ar mica ages in the External Crystalline Massifs (Dempster, 1986; Soom, 1990; Leloup et al., 2005; Challandes et al., 2008). Two biotite K–Ar results from the Aiguilles Rouges and Gastern Massifs have retained Permian ages, while one biotite/chlorite mixture has a partially reset K–Ar age of 41 Ma (Soom, 1990). Coarse-grained white mica with minor chlorite from the Gastern Massif gave Permian ages for most of the $^{40}Ar/^{39}Ar$ heating steps (Kirschner et al., 2003) and one biotite sample from the Aar Massif analysed by Soom (1990) gave a K–Ar age of 178 Ma. Similarly, Leloup et al. (2005) obtained variable

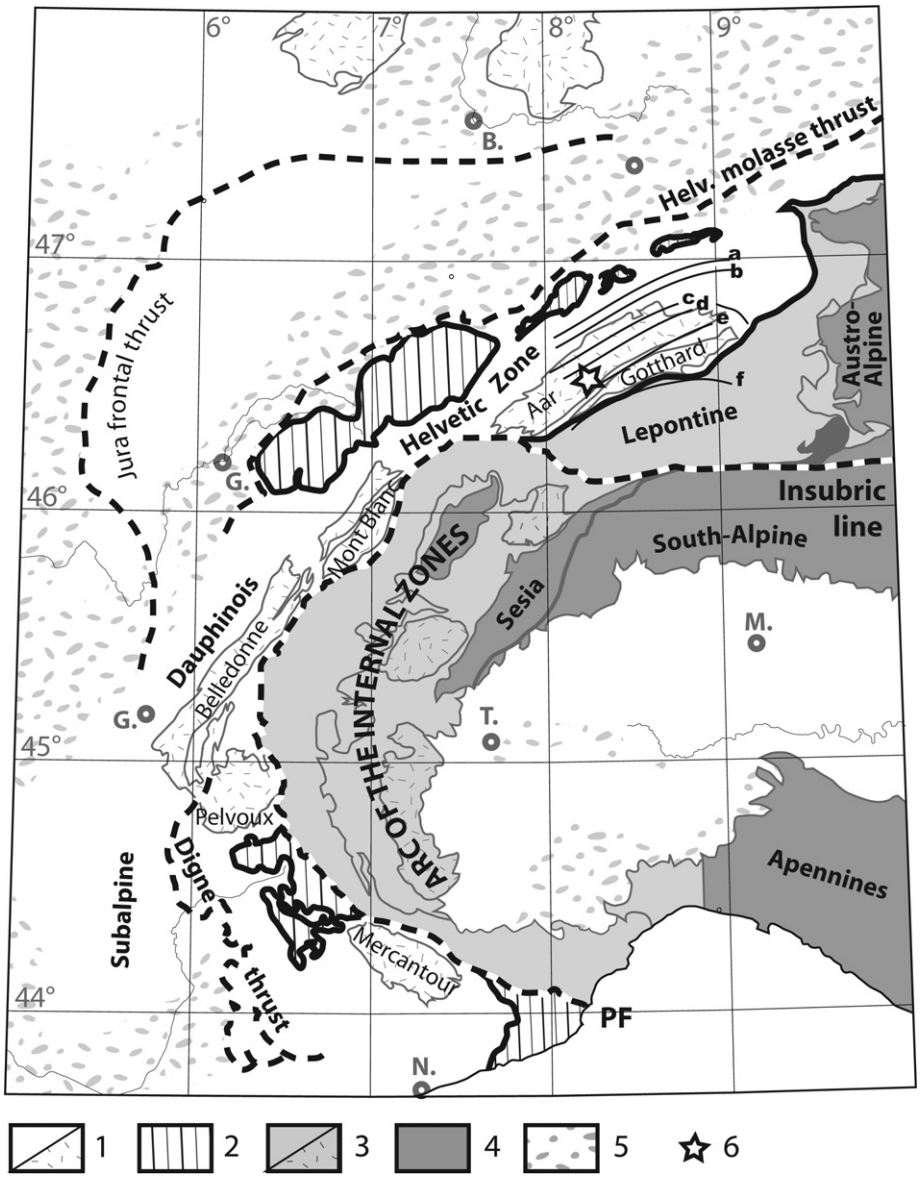

Fig. 1. Simplified geological map of the central and western Alps and of the Aar Massif, with location of the study area. External Alps comprise: 1, the Dauphinois zone, rimmed by the Jura and Alpine frontal thrusts. The Dauphinois (or Helvetic) zone comprised of a Hercynian crystalline basement (stripped) and its para-autochthonous and allochtonous Mesozoic sedimentary cover (white); 2, the transported klippes of Helminthoid Upper Cretaceous flysch and Internal Briançonnais and Penninic units. Internal Alps comprise: 3, Briançonnais and Piemontais zones, which are made of variably metamorphosed rocks from the continental European margin and the Alpine Tethys oceanic domain; 4, the Austro-Alpine units comprising the Dent Blanche klippe and the Apulian margin. Molasse sediments (5) deposited during the Oligocene to Pliocene lie in the periphery of the Alps. 6, Location of the Grimsel Pass study area. a–f, Metamorphic isograds defined by Frey (1987): a, stilpnomelane-in; b, pyrophyllite-in; c, limit between zircon mixed ages (north) and zircon cooling ages reset during Alpine orogenesis (south of line); d, stilpnomelane-out; e, chloritoid-in; f, staurolite-in.

$^{40}Ar/^{39}Ar$ biotite-plateau ages between 23 and 64 Ma in the Mont Blanc Massif. These older K–Ar and $^{40}Ar/^{39}Ar$ mica ages indicate that Alpine heating and/or recrystallisation were generally insufficient to reset the biotite and white mica K–Ar systems in areas outside Alpine shear zones. In the study area, Dempster (1986) showed that in the northern part of the Aar Massif the biotite K–Ar ages in relatively undeformed to weakly foliated granitoids systematically decrease from 245 to 67 Ma toward the centre of the massif (corresponding approximately to the stilpnomelane-out isograd, Fig. 1). In the southern part of the massif, in the Grimsel Pass area, all of the biotite and white mica dates from Dempster (1986) are in the range 10–20 Ma. This pattern is also reflected by the variable K–Ar biotite ages obtained by Michalski and Soom (1990), from 300 Ma in the less metamorphosed zones (i.e. similar to the Late Variscan granite U–Pb ages of Bussy and von Raumer, 1994) down to 17.2 Ma in the Grimsel Pass area. Michalski and Soom (1990) also noted that biotite K–Ar ages are systematically older than white mica ages in the same localities, which, for cooling ages, would be inconsistent with biotites having a lower K–Ar system closure temperature than white mica (Harrison et al., 1979).

Understanding the geological significance of mica K–Ar and Ar–Ar ages in Alpine shear zones therefore requires the integration of both structural and geochronological work, in particular to distinguish between cooling ages and formation ages that could reflect recrystallisation during deformation or isotopic resetting and/or neo-crystallisation during fluid circulation (e.g. Rolland et al., 2007, 2008; Simon-Labric et al., 2009). In the Grimsel Pass

area, it appears that several stages of shear zone formation and fluid circulation have occurred. In apparently early shear zones (below referred to as Stage 1), Challandes et al. (2008) obtained complex Ar–Ar age patterns indicating some inheritance and recrystallisation in the range of 17–21 Ma. In contrast, Rb–Sr ages of 12–10 Ma were obtained from the same shear zones (Challandes et al., 2008), which these authors interpreted as dating a late post-deformation hydrothermal event within the shear zone network (below, we refer to this event as Stage 2). Later brittle–ductile offset and reactivation of shear zones (below referred as Stage 3) are further constrained by K–Ar ages between 9 and 5 Ma (Kralik et al., 1992). Finally, brittle faulting, which in part reactivated earlier ductile shear zones and produced hydrothermally mineralized breccias, has continued in the Grimsel Pass area until at least mid-Pliocene (3.3 ± 0.06 Ma; Ar–Ar age on late-stage adularia, Hoffmann et al., 2004).

3. Sampling and analytical techniques

Mapping of the shear zone network was undertaken on the basis of several field campaigns and with the help of aerial photographs. As discussed in Section 4, this allowed several stages of shear zone formation and faulting to be recognised. Samples for Ar–Ar dating of phengite were collected from Stage 2 shear zones. One sample of biotite from an earlier Stage 1 shear zone was also analysed, which allows direct comparison with the Ar–Ar results of Challandes et al. (2008).

Electron Microprobe Analysis (EMPA) showed that phengite compositions are relatively homogeneous at a sample scale. Analyses were undertaken at the Australian National University, using a Cameca SX100 electron microprobe, using a 15 kV and 1 nA beam current, with natural samples as standards. Results are presented in Table 1.

Syn-kinematic micas separated from the selected samples (locations are shown in Fig. 2 and the Swiss coordinates given in Table 2) were analysed by $^{40}Ar/^{39}Ar$ generally using a laser to induce step-wise Ar release, but in one specific case furnace step heating was used (Section 5). Results are presented in Table 3. For mica beard aggregates, which were typically ~500 μm long with a ~10 μm grain size, separation was undertaken by careful hand-picking under a binocular microscope, to select purest phengite grains devoid of any inclusions (following the approach detailed in Rolland et al., 2008). Samples were then irradiated in the nuclear reactor at McMaster University (Hamilton, Canada), in position 5c, along with Hb3gr hornblende as a neutron fluence monitor, for which an age of 1072 Ma is adopted (Turner et al., 1971). The total neutron flux density during irradiation was 9.0×10^{18} neutron cm^{-2}. The estimated error on the corresponding $^{40}Ar^{*}/^{39}Ar_K$ ratio is $\pm 0.2\%$ (1σ).

Table 1
Representative phengite and biotite analyses from Grimsel Pass shear zones.

Mineral	Phengite					Biotite	
Sample	Aa0322	Aa0351	S70	S71	S123	Aa0350	Aa0365
SiO_2	43.95	46.02	46.96	48.03	47.41	34.74	35.08
TiO_2	0.60	0.28	0.33	0.25	0.27	1.81	1.81
Al_2O_3	23.82	26.88	28.37	27.92	27.91	15.13	15.54
FeO	8.18	5.56	4.54	4.62	4.94	23.10	22.43
MnO						0.55	0.52
MgO	3.00	1.89	1.65	1.95	1.84	8.03	8.36
CaO	0.37	0.28	0.26	0.28	0.33	0.29	0.31
Na_2O							
K_2O	10.31	10.50	10.45	10.48	10.22	9.37	9.56
Total	90.23	91.41	92.56	93.53	92.92	93.02	93.61
Mineral formulae on the basis of 22 oxygens							
Si	6.63	6.66	6.63	6.70	6.68	6.00	5.98
Al IV	1.37	1.34	1.37	1.30	1.32	2.00	2.02
Al VI	2.87	3.24	3.35	3.29	3.31	1.08	1.10
Fe^{2+}	1.03	0.67	0.54	0.54	0.58	3.34	3.20
Mg	0.67	0.41	0.35	0.41	0.39	2.07	2.12
Ti	0.07	0.03	0.04	0.03	0.03	0.24	0.23
Mn	–	–	–	–	–	0.08	0.08
K	1.98	1.94	1.88	1.87	1.84	2.07	2.08
Ca	0.06	0.04	0.04	0.04	0.05	0.05	0.06
Na	–	–	–	–	–	–	–
XFe	0.61	0.62	0.61	0.57	0.60	0.62	0.60
Si^{4+}	3.32	3.33	3.32	3.35	3.34	3.00	2.99
Ca/K	0.03	0.02	0.02	0.02	0.03	0.02	0.03

Analyses of individual mica aggregates (~0.5 mg on average) were made by step heating with a 50 W CO_2 Synrad 48-5 continuous laser beam. Measurement of isotopic ratios was done with a VG3600 mass spectrometer, equipped with a Daly detector system. Detailed procedures are given in Jourdan et al. (2004). Typical blank values for extraction and purification of the laser system are in the range 4.2–8.75, 1.2–3.9, and 2–6 cc STP for masses 40, 39 and 36, respectively.

Analysis of sample Aa0350 Biotite was undertaken with a furnace step-heating technique using a double-vacuum high-frequency furnace and a mass spectrometer composed of a 120° M.A.S.E.E. tube, a Baur–Signer GS98 source and a Blazers electron multiplier. Heating lasted 20 min for each temperature step, followed by 5 min for clean-up of the released gas, before introducing the gas into the spectrometer. Ar isotopes were of the order of 100–2000, 100–1000 and 2–200 times the blank for masses 40, 39 and 36, respectively.

All measurements were undertaken at the University of Nice (Géosciences Azur). For both Ar dating techniques, the mass-discrimination was monitored by regularly analysing air pipette volume. Decay constants are those of Steiger and Jäger (1977). As usual, uncertainties on apparent ages are given at the 2σ level and do not include the error on the $^{40}Ar^{*}/^{39}Ar_k$ ratio of the monitor.

The criteria generally used in the laboratory for defining a 'plateau' age are the following (e.g. McDougall and Harrison, 1999): (1) it should contain at least 70% of total ^{39}Ar released; (2) there should be at least three successive step-heating fractions in the plateau; (3) the integrated age of the plateau (weighted average of apparent ages of individual fractions comprising the plateau) should agree with each apparent age of the plateau within 2σ error. In this study, we also consider plateaux smaller than 70% of total ^{39}Ar, because the lower temperature age spectra are generally lowered by an Ar loss effect or by the superposition of several mineral generations. These are referred to as 'small plateau' ages.

4. Structural analysis of the Grimsel Pass shear zone network

Field relationships have been used to map and analyze the distribution, geometry, kinematics and relative chronology of shear zones in the Grimsel Pass area (Figs. 2–4). This work indicates that three major sets of shear zones (Stage 1–3) are developed. This relative timing is tested further by new Ar–Ar dating of the shear zone stages, which complements already published data.

4.1. Structural features of the superposed shear zone stages

The crystalline basement of the southern Aar Massif is made of intrusive Hercynian rocks extensively deformed during the Alpine orogeny. Foliation associated with the high-grade Alpine metamorphic event (below referred to as Stage 1 shear zones) is pervasively developed across the Grimsel Pass area. It is almost

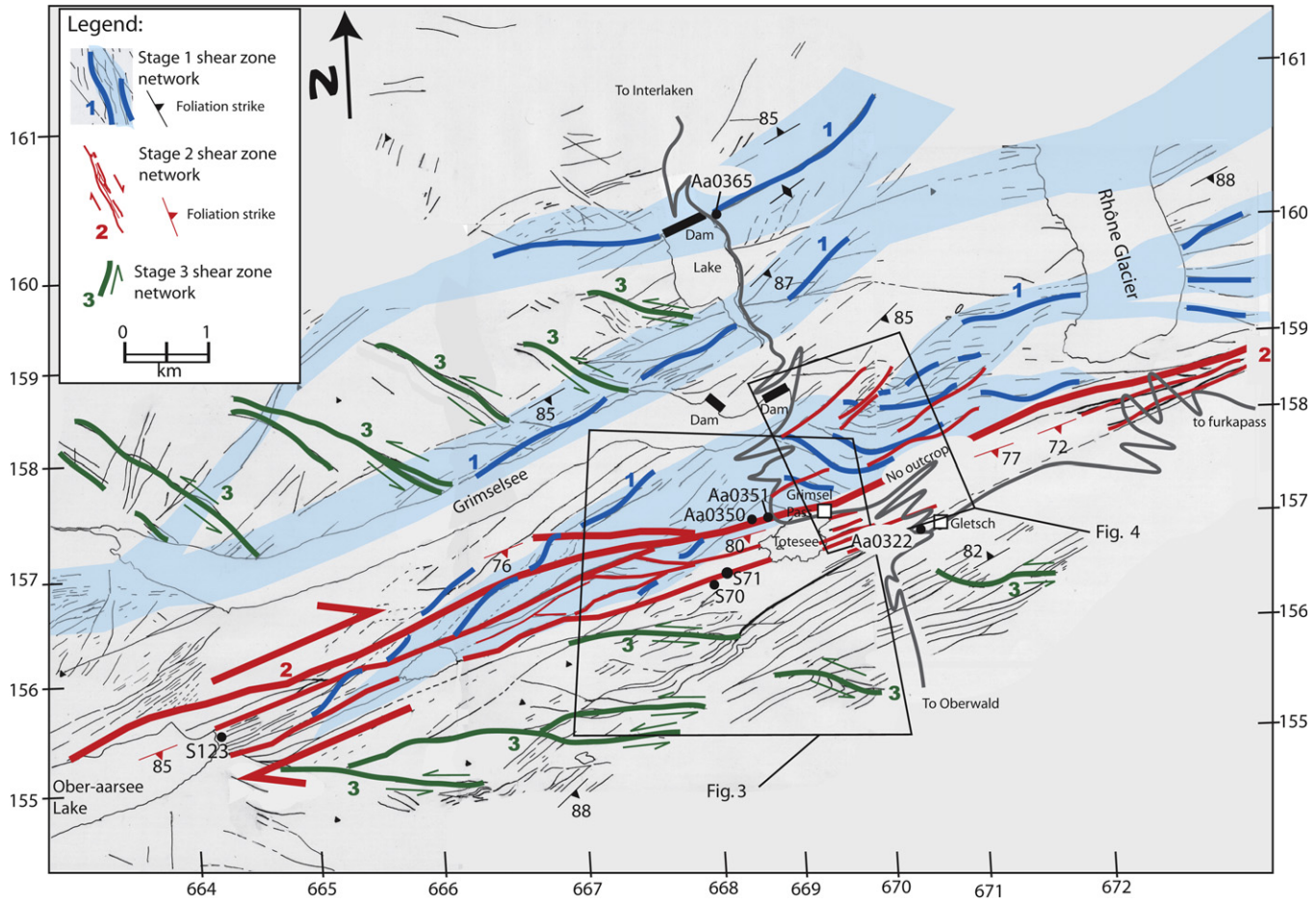

Fig. 2. Shear zone network mapped in the southern central part of the Aar Massif. Three age groups of shear zones (Stages 1–3) are distinguished. The thin grey lines on the map are highly foliated shear zones recognised from air photo interpretation. Field mapping on these features indicates that many of these zones are Stage 1 shear zones. Stage 1 shear zones represent the mylonitic cores of broad deformation zones producing a rather pervasive foliation in the area. In contrast, based on orientation and field observations, the Stage 2 and Stage 3 shear zones appear to be continuous on air photos and in the field. The location of Figs. 3 and 4 is indicated. Coordinates refer to the Swiss national metric grid and numbers refer to sample names.

vertical and shows considerable variation in strike, in the range 040–100°, but most commonly trends ca. ENE (e.g. Fig. 4). Strain is concentrated mainly in the cores of shear zones where mylonitic fabrics are developed. These high-strain zones are represented as thick blue lines in the map of Fig. 2. The mineral stretching lineation in the mylonites is steeply plunging and the sense of shear, as determined both in the field (especially from the asymmetry of S–C and S–C′ fabrics) and in thin section, alternates between top-to-north and top-to-south (e.g. Figs. 5B and 6). The mineralogy of the Stage 1 shear zones is biotite – phengite ± epidote, which developed at the expanse of Hercynian feldspars and biotite.

Stage 2 shear zones are more localised and mainly phengite-bearing. They also dip steeply (on average ~80° to the south). They are subparallel, anastomosing structures striking ~070° and concentrated in a "belt" a few hundred metres wide, with individual zones corresponding to very striking topographic depressions in the landscape (Fig. 5A). The mineral stretching lineation (commonly outlined by elongate phengite grains) is generally sub-horizontal in the central part of the Stage 2 shear zone network, whereas it becomes subvertical toward its southern rim (Fig. 6). The shear sense in the dip-slip zones is generally top-to-north. The strike-slip structures have a dextral sense (as determined by S–C and S–C′ fabrics, asymmetric intrafolial folds, and quartz microstructures: Fig. 5C–E). In the vicinity of individual Stage 2 shear zones, and particularly toward the southern part of the belt of Stage 2 shear zones, the Stage 1 foliation and mylonitic shear zones are bent into the 070° strike direction (Figs. 2–4) and are rather pervasively phyllonitized. In the area immediately east of the Grimsel Pass (Fig. 4), dominantly strike-slip dextral Stage 2 shear zones form a nearly parallel set striking 070°, which cross-cuts a more irregular network of Stage 1 shear zones and locally folded Stage 1 main foliation.

The northern rim of the Stage 2 shear zone network, and locally its southern side near the NE corner of Totesee, is marked by a zone of cataclasis which includes fault breccias (of variable thickness, from 1 to 10 m) with a biotite-rich matrix. This brittle fault zone predates Stage 2 ductile shearing, as is seen from localisation of small-scale ductile shear zones on biotite-rich brittle precursor fractures and breccia matrix on this northern rim, where the overall amount of Stage 2 brittle shearing is relatively small.

The Stage 3 shear zone network consists of more discrete brittle fracture zones. Both sinistral and dextral brittle faults are found in

Table 2
Coordinates of samples dated with the Ar–Ar method (according to the Swiss Grid).

Aa0322	E670.48	N157.05	S70	E668.27	N156.62
Aa0350	E668.66	N157.25	S71	E668.11	N156.72
Aa0351	E668.81	N157.29	S123	E664.24	N155.48
Aa0365	E668.40	N160.33			

Table 3
Phengite and biotite $^{40}Ar/^{39}Ar$ dating results from the Aar shear zones. The two distinct *J* values correspond to two different irradiations.

Sample No	Step	Laser power/Step temperature (mW/°C)	Atmospheric cont (%)	^{39}Ar (%)	$^{37}Ar_{Ca}/^{39}Ar_K$	($\pm1\sigma$)	$^{40}Ar^*/^{39}Ar_K$	($\pm1\sigma$)	$^{38}Ar_{Cl}/^{39}Ar_K$	($\pm1\sigma$)	Age (Ma) $\pm 1\sigma$
Aa0322		Phengite	$J=4.120$ (1.0%)								
	1	385	16.69	6.86	0.003	0.0002	1.69	0.030	0.014	0.0023	11.53 ± 0.21
	2	442	3.83	11.23	0.001	0.0001	1.77	0.019	0.013	0.0015	12.11 ± 0.13
	3	462	5.57	21.49	0.001	0.0001	1.88	0.012	0.013	0.0013	12.81 ± 0.08
	4	478	4.40	21.54	0.002	0.0001	1.92	0.010	0.013	0.0087	13.10 ± 0.07
	5	490	5.28	9.87	0.001	0.0001	1.93	0.019	0.013	0.0011	13.15 ± 0.13
	6	515	4.54	11.33	0.001	0.0001	1.97	0.017	0.013	0.0017	13.43 ± 0.12
	7	550	5.96	12.26	0.003	0.0001	1.95	0.023	0.013	0.0011	13.34 ± 0.16
	8	800	16.91	5.42	0.010	0.0003	2.01	0.039	0.013	0.0025	13.71 ± 0.27
Aa0350		Biotite	$J=4.147$ (1.0%)								
	1	650	1038.44	0.07	–	–	5.42	4.550	0.0701	0.0018	36.54 ± 30.34
	2	750	–	2.16	0.048	0.007	41.90	0.750	0.0196	0.0052	264.87 ± 4.44
	3	850	–	2.29	0.011	0.005	11.34	0.160	0.0179	0.0052	75.58 ± 1.03
	4	900	–	11.33	0.027	0.002	24.23	0.300	0.0167	0.0020	157.87 ± 1.89
	5	950	–	7.69	0.056	0.009	48.37	0.950	0.0156	0.0023	302.52 ± 5.49
	6	1050	–	16.08	0.090	0.021	76.91	2.170	0.0139	0.0095	459.81 ± 11.46
	7	1150	–	33.10	0.056	0.010	49.15	1.010	0.0135	0.0010	307.01 ± 5.81
	8	1250	–	13.99	0.214	0.013	178.74	11.160	0.0143	0.0013	930.17 ± 45.40
	9	1350	–	13.30	0.652	0.120	522.70	94.560	0.0165	0.0013	1965.63 ± 216.59
Aa0351		Phengite	$J=4.120$ (1.0%)								
	1	384	28.73	2.86	0.004	0.0008	1.67	0.116	0.0151	0.0051	11.38 ± 0.79
	2	415	7.25	4.98	0.002	0.0004	1.85	0.054	0.0129	0.0025	12.64 ± 0.37
	3	440	2.90	7.01	0.001	0.0001	1.95	0.040	0.0130	0.0022	13.33 ± 0.27
	4	463	1.05	14.20	0.001	0.0001	2.00	0.017	0.0128	0.0017	13.63 ± 0.12
	5	483	0.88	22.78	0.001	0.0001	2.00	0.009	0.0131	0.0015	13.66 ± 0.07
	6	494	1.65	10.98	0.001	0.0001	2.01	0.029	0.0127	0.0018	13.71 ± 0.20
	7	515	2.52	10.65	0.004	0.0002	1.99	0.024	0.0129	0.0016	13.58 ± 0.17
	8	550	0.60	26.53	0.002	0.0002	2.05	0.008	0.0128	0.0094	14.00 ± 0.06
Aa0365		Biotite	$J=4.120$ (1.0%)								
	1	382	99.03	0.03	0.019	0.0012	2.44	3.940	0.240	0.0071	16.71 ± 26.91
	2	410	73.04	2.44	0.005	0.0007	3.30	0.115	0.043	0.0032	22.61 ± 0.79
	3	419	61.90	22.80	0.003	0.0003	3.07	0.060	0.040	0.0098	20.99 ± 0.41
	4	448	21.36	17.53	0.001	0.0002	3.12	0.017	0.038	0.0013	21.35 ± 0.12
	5	460	17.12	8.55	0.002	0.0002	3.14	0.016	0.038	0.0015	21.52 ± 0.11
	6	475	16.95	4.78	0.001	0.0001	3.12	0.016	0.038	0.0015	21.38 ± 0.11
	7	490	17.20	4.58	0.001	0.0001	3.08	0.017	0.037	0.0016	21.07 ± 0.12
	8	500	17.85	8.16	0.002	0.0002	3.09	0.017	0.037	0.0016	21.18 ± 0.12
	9	510	16.88	8.64	0.001	0.0001	3.08	0.017	0.038	0.0013	21.12 ± 0.12
	10	520	17.10	7.28	0.001	0.0001	3.05	0.017	0.037	0.0014	20.90 ± 0.12
	11	550	20.49	5.00	0.003	0.0004	3.05	0.024	0.038	0.0012	20.88 ± 0.17
	12	800	22.24	10.21	0.005	0.0007	3.06	0.017	0.040	0.0011	20.95 ± 0.12
S70		Phengite	$J=51.640$ (0.2%)								
	1	367	117.57	0.11	0.025	0.00004	–	–	–		0.00 ± 0.00
	2	403	50.31	0.85	0.023	0.00004	0.37	0.098	0.0885	0.0035	10.53 ± 2.77
	3	420	22.61	1.97	0.031	0.00003	0.40	0.043	0.0237	0.0008	11.15 ± 1.22
	4	430	6.29	3.85	0.038	0.00003	0.44	0.020	0.0134	0.0002	12.46 ± 0.57
	5	434	3.72	1.96	0.041	0.00003	0.44	0.039	0.0127	0.0002	12.45 ± 1.10
	6	440	8.71	1.74	0.039	0.00002	0.41	0.044	0.0124	0.0002	11.60 ± 1.24
	7	446	0.40	1.65	0.035	0.00003	0.45	0.046	0.0125	0.0002	12.80 ± 1.31
	8	451	0.00	2.52	0.038	0.00002	0.45	0.030	0.0128	0.0003	12.84 ± 0.86
	9	457	0.00	3.01	0.041	0.00003	0.45	0.024	0.0126	0.0002	12.81 ± 0.68
	10	462	9.43	4.38	0.053	0.00002	0.41	0.014	0.0125	0.0009	11.54 ± 0.40
	11	470	6.55	4.90	0.061	0.00003	0.42	0.014	0.0125	0.0001	11.97 ± 0.39
	12	478	0.87	6.39	0.047	0.00005	0.45	0.012	0.0126	0.0002	12.82 ± 0.36
	13	486	2.27	11.20	0.045	0.00004	0.46	0.007	0.0128	0.0002	12.89 ± 0.21
	14	490	2.93	12.88	0.083	0.00006	0.45	0.005	0.0126	0.0001	12.66 ± 0.16
	15	494	2.64	6.35	0.080	0.00003	0.45	0.009	0.0128	0.0009	12.82 ± 0.26
	16	500	3.07	11.84	0.373	0.00001	0.46	0.006	0.0125	0.0004	13.02 ± 0.18
	17	507	2.80	15.01	0.156	0.00006	0.46	0.004	0.0127	0.0004	13.10 ± 0.13
	18	514	0.00	0.89	0.163	0.00008	0.50	0.087	0.0131	0.0004	14.08 ± 2.45
	19	528	0.00	0.91	0.275	0.00001	0.52	0.063	0.0121	0.0004	14.62 ± 1.79
	20	553	0.00	0.70	0.625	0.00003	0.55	0.109	0.0133	0.0006	15.57 ± 3.05
	21	601	19.60	0.64	3.002	0.00002	0.41	0.082	0.0137	0.0008	11.67 ± 2.30
	22	800	2.34	6.22	0.487	0.00002	0.47	0.008	0.0125	0.0008	13.34 ± 0.25
S71		Phengite	$J=51.400$ (0.2%)								
	1	450	11.66	13.13	0.040	0.00002	0.43	0.007	0.428	0.002	12.17 ± 0.20
	2	470	5.72	6.69	0.038	0.00002	0.42	0.010	0.416	0.001	11.84 ± 0.29
	3	486	3.04	7.45	0.051	0.00002	0.43	0.011	0.432	0.001	12.29 ± 0.32
	4	499	1.80	9.47	0.049	0.00002	0.45	0.011	0.447	0.001	12.71 ± 0.32

Table 3 (*continued*)

Sample No	Step	Laser power/Step temperature (mW/°C)	Atmospheric cont (%)	^{39}Ar (%)	$^{37}Ar_{Ca}/^{39}Ar_K$	($\pm1\sigma$)	$^{40}Ar^*/^{39}Ar_K$	($\pm1\sigma$)	$^{38}Ar_{Cl}/^{39}Ar_K$	($\pm1\sigma$)	Age (Ma) $\pm 1\sigma$
	5	513	1.56	15.96	0.063	0.00003	0.46	0.006	0.457	0.001	13.00 ± 0.17
	6	535	1.51	23.92	0.183	0.00007	0.46	0.005	0.463	0.006	13.17 ± 0.14
	7	574	0.00	15.59	0.076	0.00003	0.48	0.006	0.477	0.003	13.55 ± 0.20
	8	800	1.91	7.79	0.523	0.00003	0.47	0.011	0.466	0.003	13.25 ± 0.33
S123 (1)		Phengite	$J = 51.400$ (0.2%)								
	1	382	27.78	3.15	0.004	0.0003	0.38	0.090	0.014	0.001	10.65 ± 0.28
	2	397	11.23	1.59	0.003	0.0006	0.40	0.018	0.013	0.001	11.45 ± 0.52
	3	412	10.01	2.42	0.004	0.0006	0.40	0.011	0.013	0.001	11.32 ± 0.32
	4	421	12.09	1.91	0.005	0.0004	0.38	0.015	0.013	0.001	10.77 ± 0.42
	5	429	5.08	2.84	0.005	0.0007	0.41	0.012	0.013	0.001	11.60 ± 0.35
	6	439	7.92	2.99	0.006	0.0006	0.39	0.008	0.013	0.001	11.17 ± 0.25
	7	450	3.67	2.88	0.004	0.0005	0.41	0.009	0.013	0.001	11.69 ± 0.26
	8	462	5.06	2.83	0.003	0.0004	0.41	0.010	0.013	0.001	11.51 ± 0.29
	9	470	2.72	4.22	0.003	0.0004	0.42	0.006	0.013	0.001	11.85 ± 0.19
	10	480	4.32	4.65	0.002	0.0002	0.41	0.005	0.013	0.001	11.76 ± 0.16
	11	490	1.74	6.10	0.002	0.0002	0.43	0.005	0.013	0.001	12.16 ± 0.16
	12	499	2.36	6.73	0.002	0.0002	0.43	0.004	0.013	0.001	12.14 ± 0.13
	13	506	0.73	10.13	0.001	0.0002	0.44	0.002	0.013	0.001	12.48 ± 0.10
	14	511	0.23	7.76	0.002	0.0002	0.45	0.004	0.013	0.001	12.66 ± 0.14
	15	517	0.80	14.85	0.002	0.0009	0.45	0.002	0.013	0.001	12.73 ± 0.08
	16	520	2.90	9.59	0.003	0.0003	0.44	0.004	0.013	0.001	12.49 ± 0.11
	17	525	6.98	2.16	0.004	0.0007	0.42	0.016	0.012	0.001	11.98 ± 0.46
	18	800	2.38	13.20	0.008	0.0003	0.44	0.002	0.012	0.001	12.56 ± 0.08
S123 (2)		Phengite	$J = 51.310$ (0.2%)								
	1	420	27.12	11.40	0.005	0.00007	0.37	0.014	0.015	0.003	10.38 ± 0.42
	2	473	4.65	11.43	0.005	0.00008	0.41	0.012	0.013	0.002	11.52 ± 0.36
	3	515	2.31	16.76	0.005	0.00007	0.42	0.012	0.012	0.002	11.88 ± 0.36
	4	535	6.48	11.66	0.010	0.00008	0.41	0.012	0.013	0.001	11.58 ± 0.34
	5	560	1.20	41.38	0.003	0.00002	0.44	0.004	0.013	0.001	12.56 ± 0.12
	6	750	0.00	7.37	0.008	0.00009	0.46	0.019	0.013	0.002	12.97 ± 0.54

outcrop. Dextral brittle faults have a strike close to that of the Stage 2 mylonitic foliation (i.e. ~070°, Fig. 6), whereas sinistral faults are slightly oblique (120°–130°). Offsets are visible on 090° Stage 3 shear zones, but no offsets are apparent on the 120–130 set (Fig. 2).

4.2. Microstructure of shear zones and sample description

The shear zone network investigated in this study is developed within the Grimsel granodiorite. The locally preserved protolith granodiorite consists of centimetre-sized crystals of plagioclase (~20–30%) in a matrix of quartz (~30–40%), biotite (~10–15%), and minor K-feldspar (~5–10%).

Stage 1 shear zones are typically enriched in biotite. In thin section, the Stage 1 shear zones consist of finely recrystallized (<500 μm) biotite + phengite + epidote aggregates around feldspar porphyroclasts. These zones do not show any sign of late alteration or tectonic reactivation. For instance, biotite is not chloritized, and no features of superposed deformation could be seen within the samples.

Stage 2 shear zones are mostly phengite-rich. In thin section (Fig. 7), they exhibit very fine-grained (generally <250 μm) aggregates of phengite that develop at the expense of biotite and feldspars. Cloudy patches of sphene and oxides are found as a result of biotite breakdown. On the microscopic scale, progressive deformation is accompanied by increasing alteration of feldspar porphyroclasts into phengite. Micro-scale observations indicate progressive deformation within a single deformation phase. Neocrystallised phengite is not deformed and no clasts of previously crystallised phengite were found transposed into the main foliation. Secondary chloritisation is common. Si contents in phengites (Si 3.32–3.35) are similar to those of Stage 1 phengite (Si 3.20–3.31; Challandes et al., 2008), consistent with recrystallisation at a similar pressure range (around 0.6 GPa, see Geological Setting; Table 1).

Stage 3 shear zones and faults are brittle–ductile. In thin section, the typical observed assemblage is chlorite + quartz, and no phengite is present.

5. $^{40}Ar/^{39}Ar$ dating of shear zone minerals

Dating results for shear zone samples are shown in Figs. 8 and 9 and listed in Table 3. All the $^{40}Ar/^{39}Ar$ spectra from mylonite samples gave plateau (or small plateau) ages at the 2σ level. In most samples, there is a slight staircase shape, with low temperature steps having lower ages (Fig. 8). These patterns could be ascribed to partial ^{40}Ar loss in phengite, possibly due to fluid percolation through shear zones after initial mylonitization, as has been proposed for similar examples from other External Crystalline Massifs in the Alps (Rolland et al., 2007, 2008). It follows that if the high temperature steps of the phengite $^{40}Ar/^{39}Ar$ spectra represent a small plateau age, then it should correspond to a minimum age that may be close to the initial "undisturbed" age. Isochron ages, which can only be determined when there is sufficient spread in $^{39}Ar/^{40}Ar$ vs $^{36}Ar/^{40}Ar$ ratios, are in all cases similar within error to plateau ages. In addition, initial $(^{36}Ar/^{40}Ar)_0$ ratios are close to the air value. This is interpreted as indicating the absence of ^{40}Ar excess in the phengite samples, unlike the biotite cataclasite sample (Aa0350, Fig. 9), which is considered in more detail below. The Ca/K ratios remain low and rather constant for all samples (Table 3). They consistently lie within the range obtained from electron microprobe analyses, suggesting that the mica separates are homogeneous despite their very small size.

Sample Aa0365 consists of biotite from a Stage 1 shear zone and was analysed for comparison with Stage 1 shear zones dated by Challandes et al. (2008). The $^{40}Ar/^{39}Ar$ spectrum shows a plateau

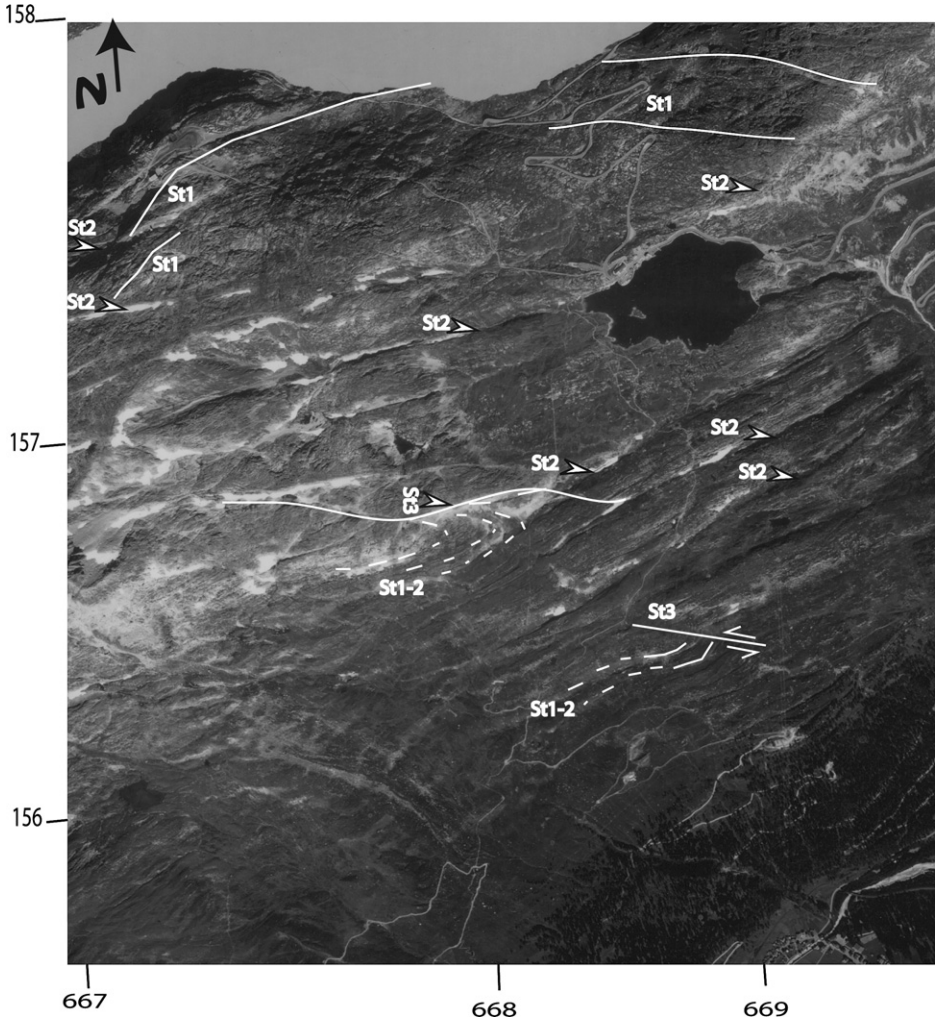

Fig. 3. Aerial photograph showing the relationships between the three shear zone networks (St1 = Stage 1; St2 = Stage 2; St3 = Stage 3). Note that in the southern part of the photo, only a single Stage 1–2 composite foliation is present, parallel to the strike of Stage 2 shear zones, whereas in the northern part the Stage 1 foliation is oblique to the strike of the main Stage 2 shear zone. Stage 3 shear zones are distinctly oblique (N90 or N120–130) to the Stage 1–2 strike, with a clear sinistral strike-slip sense. The coordinates refer to the Swiss national metric grid.

age at 21.1 ± 0.2 Ma (2σ), with 97.5% of ^{39}Ar released. The isochron age comprising all data points (21.2 ± 0.1 Ma) is effectively identical to the plateau age. This result is consistent with the results of Challandes (2001), who reported Ar–Ar ages for Stage 1 shear zones in the range 17–21 Ma.

Stage 2 mylonite shear zone samples all consist of phengite. They give ^{40}Ar/^{39}Ar spectra and inverse isochron ages in a tight range between 12.2 ± 0.2 Ma and 13.8 ± 0.1 Ma (Fig. 8). Sample Aa0351gives an age of 13.8 ± 0.1 with 70% ^{39}Ar released. The inverse isochron age of 13.7 ± 0.1 Ma is identical within error. Sample Aa0322 gives a plateau age of 13.3 ± 0.1 Ma, and an inverse isochron age of 12.7 ± 0.3 Ma. Sample S70 gives a plateau age of 12.8 ± 0.2 Ma and an inverse isochron age of 12.6 ± 0.2 Ma. Analysis of sample S71 provides a plateau age of 13.2 ± 0.2 Ma but the inverse isochron could not be calculated, due to the lack of a sufficient spread in the ^{36}Ar/^{40}Ar and ^{39}Ar/^{40}Ar ratios.

To check if the small differences in age between these samples are significant, perhaps reflecting slightly different times of activity on different Stage 2 shear zones, or the time span of progressive crystallisation within one shear zone system, duplicate analyses were made on sample S123. These duplicate analyses gave ages of 12.2 ± 0.2 Ma (2σ) and 12.6 ± 0.2 Ma (2σ), respectively. The difference of 0.4 Ma is small but still significant at the 2σ uncertainty-level.

Dating of the early Stage 2 biotite from cataclasite sample Aa0350 gave a disturbed staircased Ar spectra (Fig. 9). The biotite sample was taken from the cataclastic northern rim of the Stage 2 shear zone network (Fig. 2). The age spectra obtained show a striking staircase shape, with age values ranging between 36 and 1965 Ma. The Ca/K ratios are consistent with EMPA values. The inverse isochron plot shows a very low initial (^{36}Ar/^{40}Ar)$_0$ ratio of 4.10^{-5}. Thus, both the Ar–Ar spectrum and the inverse isochron can be interpreted as the result of a very significant excess ^{40}Ar component in the sample. However, the inverse isochron plot still provides a geologically reasonable Ar age of 15.5 ± 0.1 Ma, showing that the biotite is Alpine in age, and possibly slightly older than the phengites. This is consistent with the field observation that the biotite-filled fractures acted as precursors for subsequent Stage 2 ductile shear zone strain localisation.

6. Discussion

6.1. Significance of ^{40}Ar/^{39}Ar ages from shear zone mylonites

In all the analysed phengites, the ages obtained can be considered as 'geologically significant'. Plateau ages are generally, within error, identical to calculated inverse isochron ages. Further, the Ar_{Ca}/Ar_K

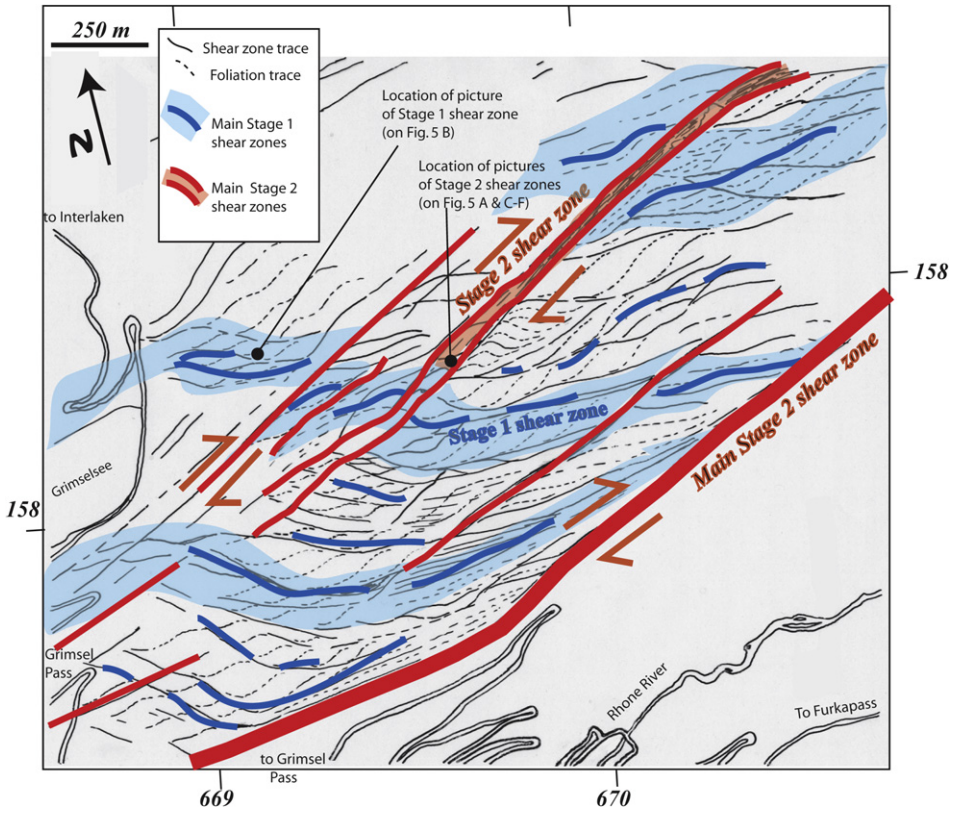

Fig. 4. Detailed shear zone map of the eastern part of the Grimsel Pass. Note the irregular pattern of Stage 1 shear zones and associated foliation, whereas Stage 2 shear zones are generally subparallel. The coordinates refer to the Swiss national metric grid.

ratios are low, and close to those obtained by EMPA. Several lines of evidence allow us to interpret the mica ages as 'crystallisation ages' following Villa et al. (1997), and not as simple 'cooling ages'. The small but significant variation in $^{40}Ar/^{39}Ar$ ages within small domains is more in agreement with slow crystallisation of phengite during this time, or to superposed crystallisation events. Furthermore, white mica ages are consistently younger than those of biotite, which is contrary to the generally accepted cooling sequence (e.g. Purdy and Jäger, 1976; Wagner et al., 1977). This is also supported by the observation that the temperature necessary for syn-kinematic growth of phengite (350–400 °C) is in the same range as the 'closure temperature' typically proposed for white mica (e.g. McDougall and Harrison, 1999).

However, ages obtained for mylonites sampled at different positions within the Stage 2 shear zone network all lie within the range 13.8 ± 0.1 Ma and 12.2 ± 0.2 Ma. This age window is narrow but larger than the 2σ uncertainty. The duplicate analyses of sample S123 also show a difference that is approximately twice 2σ. These slightly different ages obtained from the same phengite separate demonstrate that sampling at a 500 μm scale (i.e. the size of the aggregates dated by laser-Ar) still retains some $^{40}Ar/^{39}Ar$ age heterogeneity. Such heterogeneity found within a single sample at the <500 μm scale, as well as from different shear zones of similar orientation and kinematics, could be due to many factors, such as:

(1) partial Ar loss due to post-deformation fluid circulation;
(2) irregular distribution of minor amounts of excess Ar, either due to incomplete degassing during neo- or recrystallisation of phengite or introduced by fluid circulation;
(3) age differences due to sampling of different microstructural sites within the same sample, such as fibrous mica beards, the foliation-defining mica domains, or mica-filled microfractures, which developed at different times during progressive shearing;
(4) continued growth of phengite in the same structural site during the progressive shearing event.

Each of these possibilities will now be discussed in more detail.

(1) If the variability is due to Ar loss during or after the main ductile deformation phase (Kramar et al., 2001), then the older ages (or the higher temperature step) would be closer to the real deformation age. Such ^{40}Ar loss could explain the slight staircase shape observed in most spectra (Rolland et al., 2008). However, all ages reach a plateau before the middle of the spectra, and a plateau age is calculated with more than 50% and up to 98% of the ^{39}Ar. In any case, taking into account the older age step value as representative of the deformation age would make it older by only ~0.2 Ma, which is about the error value. Ar loss alone cannot therefore account for the age discrepancy between different samples.
(2) The presence of minor excess ^{40}Ar cannot be totally discarded because we are only considering rather small age differences. However, this hypothesis seems unlikely in the phengite samples from mylonites, as the inverse isochron plots show initial $(^{36}Ar/^{40}Ar)_0$ ratios relatively close to the air value (e.g. Scaillet, 1996; Arnaud and Kelley, 1995; DeJong et al., 2001).
(3) The Ar patterns could reflect mixtures and intergrowths between different generations of white mica (Villa et al., 1997) or between white mica and other phyllosilicates

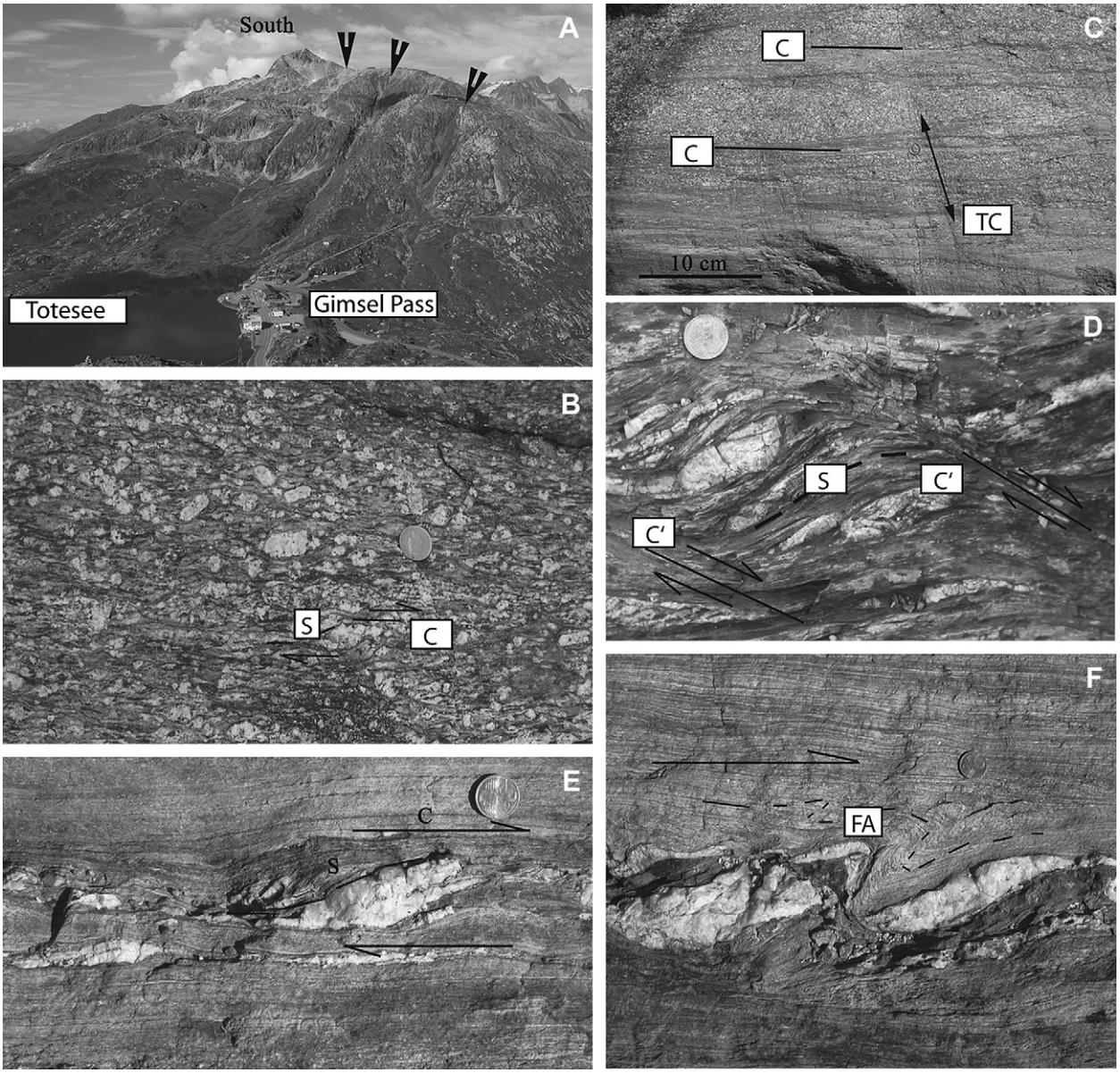

Fig. 5. Structural field relationships of Grimsel Pass shear zones (locations of pictures shown in Fig. 4). A: landscape view of the shear zone network, looking SW toward the Totesee and Grimsel Pass from the location indicated in Fig. 4, showing main (Stage 2) shear zones of Figs. 2–4 (indicated with arrows); B: S–C structures of Stage 1 shear zones, indicating a top-to-the north sense of shear on a subvertical N170 scarp (photo is rotated through 90°); C–F: phyllonitic foliation typical of Stage 2 shear zones (photographs of horizontal surfaces, the width of which is parallel to N070 direction, top of pictures is toward the north). Mineral lineations measured in the field are horizontal. Picture C: rim of Stage 2 shear zones showing intense shearing (C); "TC" refers to tensial cracks. Picture D shows S–C′ relationships, while Picture E depicts S–C relationships and Picture F shows fold asymmetry ("FA"), always consistently indicating a dextral sense of shear.

present as intergrowths, such as paragonite (Boundy et al., 1997), illite (DeJong et al., 2001) or chlorite (Lo and Onstott, 1989). The sampling of several phengite generations formed in different structural zones of the same sample is very likely as the microsampling method used cannot exclude such variability on a scale <500 μm.

(4) The age difference between different parts of the shear zone network does not exceed 2 Ma. This argues more for progressive deformation than for distinct phases, as also suggested by Müller et al. (2000a,b) for other examples from the Eastern Alps and Pyrenees. Field and microstructural observations do not provide any evidence for superimposed deformation events during Stage 2 shearing. Instead, at the outcrop scale, progressive deformation and syn-kinematic mineral transformation is observed from rim to core of the shear zones. As shown by the microstructural analysis (see Section 4.2), progressive deformation is accompanied by increasing alteration of feldspar porphyroclasts into biotite, then replaced by phengite + chlorite. These observations made from outcrop to thin-section (Fig. 7) scale show that deformation has been progressive in space and time and not multiphase. Because the deformation during Stage 2 shearing is inferred to be a short-lived (<2 Ma) continuous deformation, the change in kinematics from the core (dextral strike-slip) to the southern rim (top-to-north thrusting) of the Stage 2 shear zone network could reflect strain partitioning during overall transpressive tectonics (e.g. Tikoff and Teyssier, 1994).

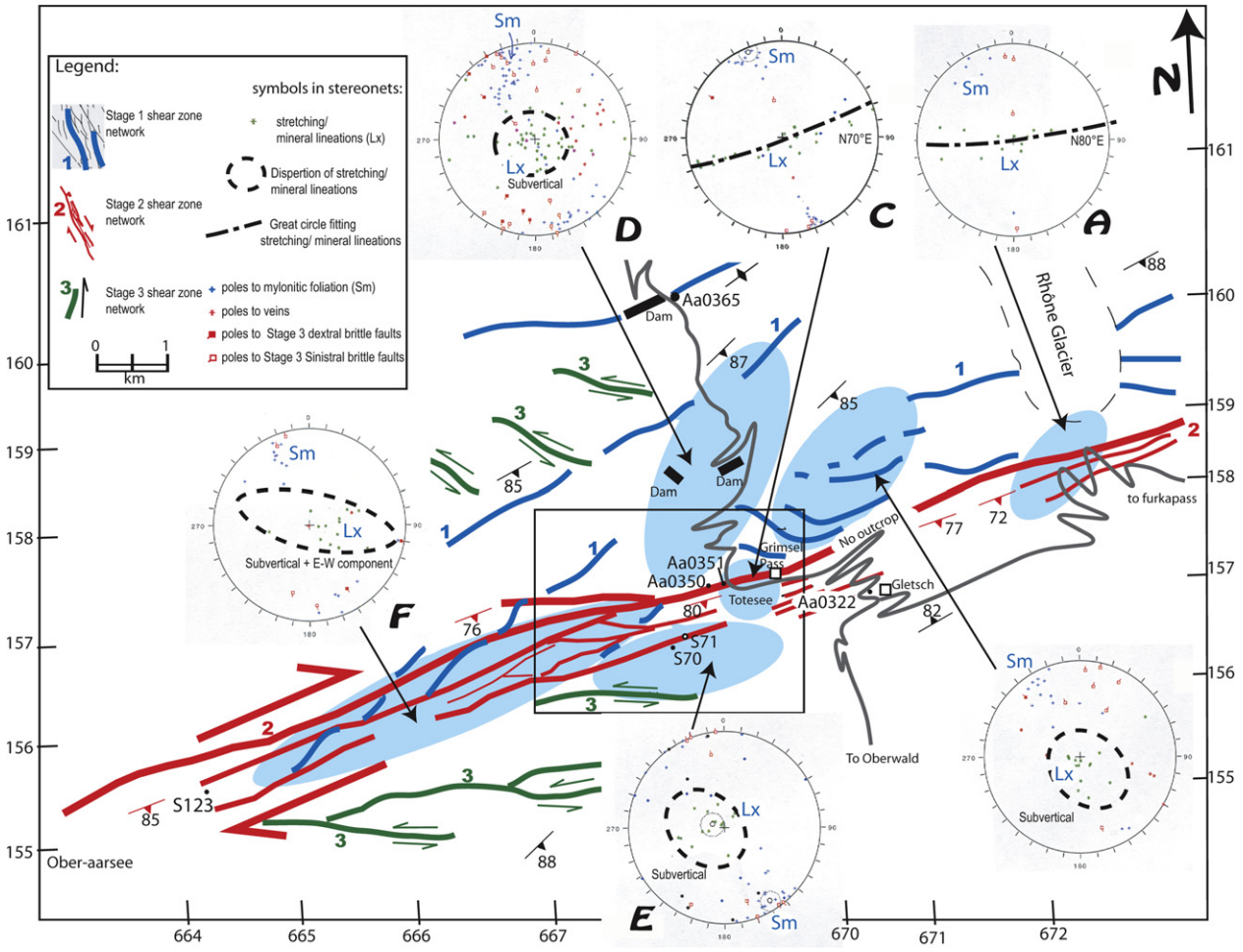

Fig. 6. Orientation data from the Grimsel Pass area. Shaded ellipses represent the area of measured data collection. Note that generally (stereonets A–E), the mylonitic foliation strike is about N070–N080. Mineral and stretching lineations, measured on these planes are generally subvertical in areas far from the main Stage 2 shear zone (stereonets B, D, E), whereas they tend to be more horizontal within the main shear zone. In some cases, lineations are more widely dispersed along great circles corresponding to the mean mylonitic foliation (stereonets A, C, F), reflecting greater variability in the pitch of the lineation. Veins are generally sub-perpendicular to the main Stage 2 shear zone (N160 on average, stereonet D). The Stage 3 shear zone network consists of sinistral and dextral brittle faults. Dextral brittle faults have a strike close to the Stage 2 mylonitic foliation, whereas sinistral faults are slightly oblique (N070–N120), so only this sinistral set appears on the map. Data are plotted in Wulff stereonets in the lower hemisphere.

6.2. Model for coupled fluid flow and deformation during Stage 2 shearing

The Stage 2 deformation in the Grimsel Pass area provides another excellent example of a deformed granitoid pluton in which precursor brittle fractures may play a crucial role in initiating fluid–rock interaction, thereby localising subsequent ductile heterogeneous shear (e.g. Segall and Simpson, 1986; Guermani and Pennacchioni, 1998; Rolland et al., 2003; Mancktelow and Pennacchioni, 2005; Pennacchioni, 2005; Pennacchioni and Mancktelow, 2007). Stage 2 shear zones appear to have been zones of more localised and discrete deformation and fluid–rock interaction in comparison to earlier Stage 1 structures. Initial deformation in Stage 2 shear zones was brittle but most displacement along the shear zones occurred during later ductile reactivation associated with reaction softening due to the development of phengite from feldspar (i.e. phyllonitization). As such, reaction softening may have been critical for the extreme localisation of Stage 2 deformation.

In the Grimsel area, it may be possible to estimate the time between initial fracturing and subsequent ductile shearing. The cataclasites preserved on the northern rim of the Stage 2 shear zone network (Fig. 10) are sealed with newly grown biotite that must have crystallised during or shortly after brittle deformation. Ar dating of this biotite resulted in two significant observations.

(1) There is considerable excess Ar in the sample, which is unusual compared to all other samples dated in this study. In general, the common explanation for excess Ar is the presence of a high ambient partial pressure of ^{40}Ar (e.g. Lovering and Richards, 1964; Foland, 1983; Roddick et al., 1980; Harrison and McDougall, 1981; Scaillet, 1996 McDougall and Harrison, 1999; Kelley, 2002). This requires conditions conducive to the introduction and retention of radiogenic ^{40}Ar within the rock. Although Roddick et al. (1980) and Cumbest et al. (1994) suggested that some excess Ar could originate from an atmospheric source and be transported and trapped in metamorphic minerals at middle crust levels, this seems unlikely in the current case because fluids likely percolated upwards. The fluids were oversaturated in silica, as shown by the presence of quartz veins, either preserved in the proximity of deformed (Fig. 5D) within the shear zones. Therefore they must originate from a source at a somewhat deeper level, as the solubility of silica is higher in HT fluids. In contrast, a relatively local source for excess Ar is more likely, consistent with the work of Foland (1979), who showed that

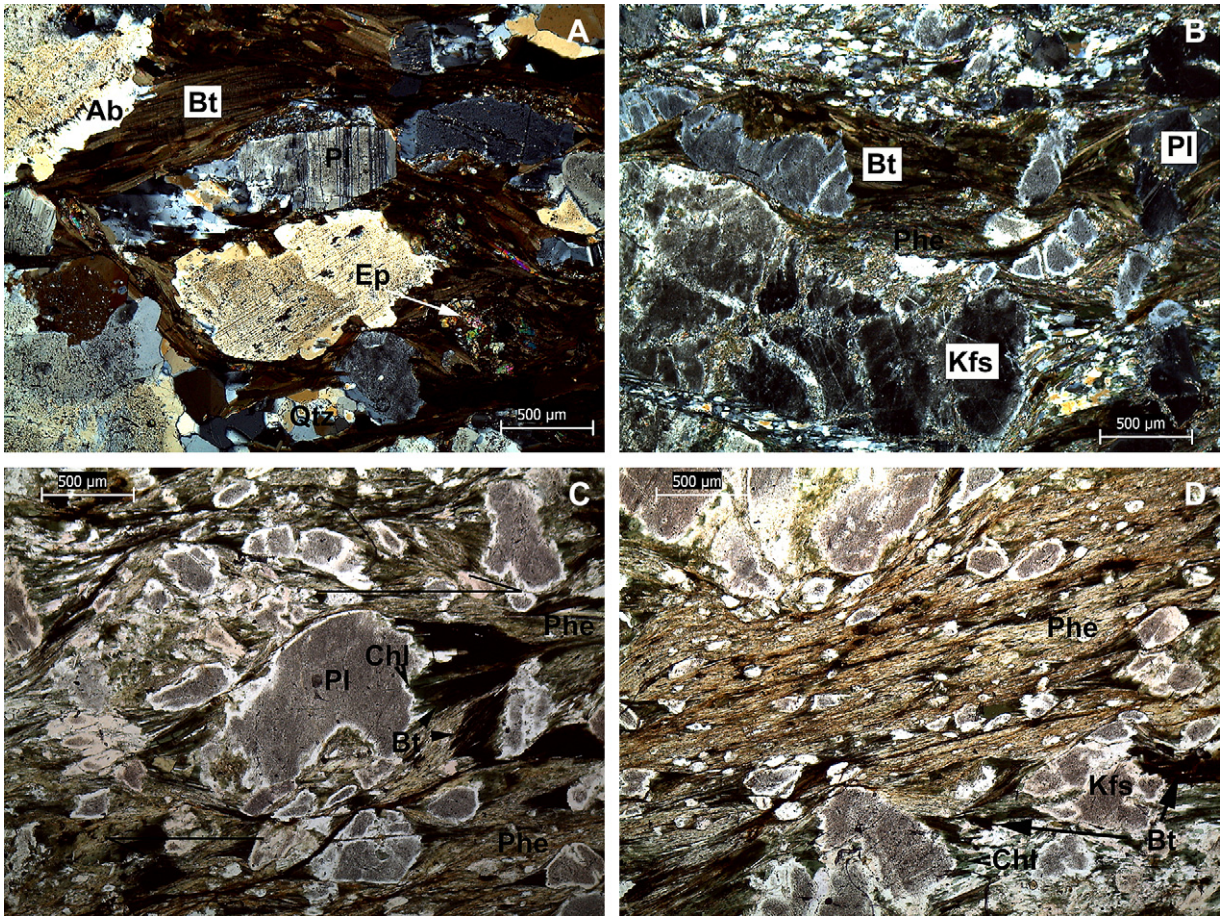

Fig. 7. Photomicrographs from representative shear zones, showing: A, picture in crossed polars of shear zone Aa0365 showing a stage 1 biotite-bearing fabric (Bt), with local patches of epidote (Ep); B, picture in crossed polars of biotite-rich cataclasite Aa0350, brittle precursor of Stage 2 mylonites; C, Phengite-rich shear zone (sample Aa0351), showing the size of the fibrous phengite (Phe) beard structures, which develop on the ends of corroded and albitized (Ab) K-feldspar clasts (Kfs) and plagioclase (Pl) clasts where they are at a high angle to the stretching direction and crystallize after the biotite (natural light). Such mica beards grow in micro-dilation sites as the matrix progressively pulls away from rigid clasts during stretching, and the fibres tend to grow parallel to the stretching direction; D, phengite-rich shear zone (sample S123), with a thick phengite band, showing some minor clasts of feldspar surrounded by biotite and chlorite (Chl) fibers (natural light). White aureoles surrounding K-feldspar are albitic zones. Thin sections orientations are perpendicular to the foliation and parallel to the main lineation. Locations of samples are shown in Fig. 2.

variable amounts of excess Ar in biotites correlate with whole rock potassium content for transects of up to ~10 m. Such relatively small-scale (centimetre-scale) Ar transfer is suggested by Scaillet (1996), and may be ascribed to "internal isotopic buffering", promoted by low intergranular diffusivities. This buffering may be due to compositional variations, as shown by Harrison and McDougall (1981). In their study, it is suggested that excess Ar released from a metamorphosed gneiss penetrated and remained within neighboring country granulites, especially close to the contact with the gneiss. Further evidence for compositional and structural controls on the distribution of excess Ar in biotites is provided by Baxter et al. (2002) at the Simplon Pass. They relate it to an intrinsic system parameter, the transmissive timescale, which is the characteristic time for Ar to escape through the local intergranular transporting medium. In their model, Baxter et al. (2002) argue that build-up of significant excess Ar is achieved when the transmissive timescale is long relative to the true closure age of the mineral, which essentially depends on the diffusivity of Ar in the matrix. However, it is clear that several fluid sources may have existed and research focussed on the origin of the fluids contained in the different shear zone types appears necessary to understand the size of fluid circulation pathways.

(2) The inverse isochron plot gives an age of ~15.5 ± 0.1 Ma for the biotite in the cataclasite (Fig. 9), which is significantly older, by about 2 Ma, than the phengite from the mylonites. Due to the disturbance of the Ar system by percolating fluids one has to be cautious about the interpretation of such an age difference. It is possible that this older age corresponds to the time of fluid circulation prior to phengite growth. The difference in age is consistent with the relative age deduced from microstructural observation that phengite appears to replace biotite along a narrow reaction zone at the margin of the ductile part of the shear zone (Fig. 10). During this period of fluid flow, fluids were enriched in Ar due to the alteration of feldspar and biotite in the granite host (e.g. Figs. 7 and 10) and the biotite matrix of the cataclasite may have served as a sink for Ar contained in the percolating fluid. It is known that excess ^{40}Ar preferentially partitions into biotite rather than muscovite (Kelley, 2002 and references therein). Otherwise this might be due to the specific nature of the fluid or due to the long time span of fluid circulation, as there was no or little muscovite present when the biotite cataclasites were being produced. In conclusion, excess Ar may be considered in the case study as one amongst several features of element transfer during cataclasis and subsequent fluid–rock interaction. The zone of excess Ar can be

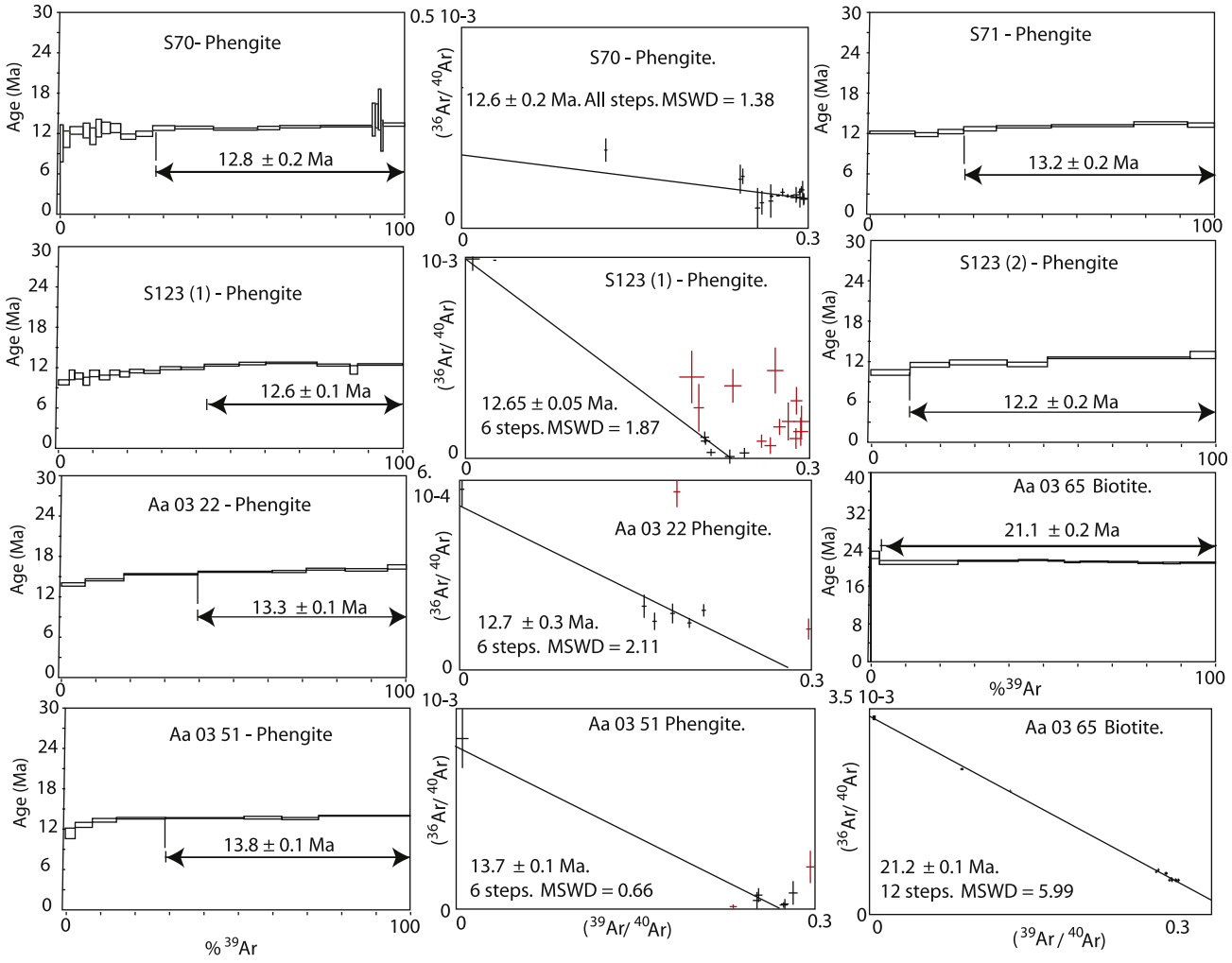

Fig. 8. $^{40}Ar/^{39}Ar$ spectra and isochron correlation diagrams for Grimsel Pass shear zone samples. In the inverse isochron plots, the same steps were used as in the (small) plateau age calculation. Note that there is a good correspondence between the two plots. For samples S71 and S123 (2), no reliable isochron age could be obtained due to the small spread in $^{40}Ar/^{36}Ar$ and $^{39}Ar/^{36}Ar$ ratio values. Locations are shown in Fig. 2 and Table 2.

correlated with a zone with distinct structural style at the shear zone rim. This cataclastic zone is bounded by phengite-bearing phyllonites in the centre of the shear zone passing with a gradual change to a quartz–feldspar–phengite mylonite at the southern rim. This transition includes a progressive rotation of the mineral/stretching lineation marked by horizontally aligned phengite observed across the main Stage 2 shear zone, which steepens toward the southern part of the shear zone. The deformation may therefore have been strongly transpressive, with only a very narrow (~10 m) zone dominated by strike-slip shearing. This would be consistent with the regional kinematics of the western and central Alps during the Neogene, as will be discussed in the next section.

6.3. Deformation history

This study using $^{40}Ar/^{39}Ar$ laser techniques on syn-kinematic mica formed in brittle–ductile high-strain zones complements previous studies undertaken using (i) the standard K–Ar technique applied to micas from undeformed host-rocks on the regional scale of the Aar and Gotthard Massifs (Michalski and Soom, 1990), (ii) the furnace step-heating $^{40}Ar/^{39}Ar$ method on biotite and phengite from Grimsel Stage 1 shear zones (Challandes, 2001; Challandes et al., 2008), and (iii) K–Ar on fault gouge minerals, which tentatively dates the late brittle history of the southern Aar Massif (Kralik et al., 1992).

The first deformation event documented in the Aar Massif is characterized by the pervasive development of a biotite-bearing foliation in the area, as well as by the localised development of biotite-bearing shear zones (Choukroune and Gapais, 1983; Marquer, 1989; Fourcade et al., 1989). Challandes et al. (2008) obtained biotite Ar-step ages mostly in the range 21–17 Ma, together with some much older (>100 Ma) steps, but did not obtain any well-defined plateau age. This variation in ages is consistent with the variable biotite K–Ar ages obtained elsewhere in the Aar Massif, which range from unreset (~300 Ma) Variscan ages down to (~20 Ma) Alpine ages (Michalski and Soom, 1990). A similar spread in $^{40}Ar/^{39}Ar$ ages was obtained in the Helvetic Nappes (Kirschner et al., 1996, 1999, 2003). This spread has been interpreted as the result of Ar inheritance, due to partial preservation of detrital Variscan mica interfingered with neo-crystallised Alpine metamorphic mica. Our biotite sample (Aa0365) from a Stage 1 shear zone gave a well-defined plateau age of 21.1 ± 0.2 Ma, perfectly corresponding with the oldest "Alpine" ages obtained by Challandes et al. (2008). This age has some important implications for the deformation history of the Aar Massif:

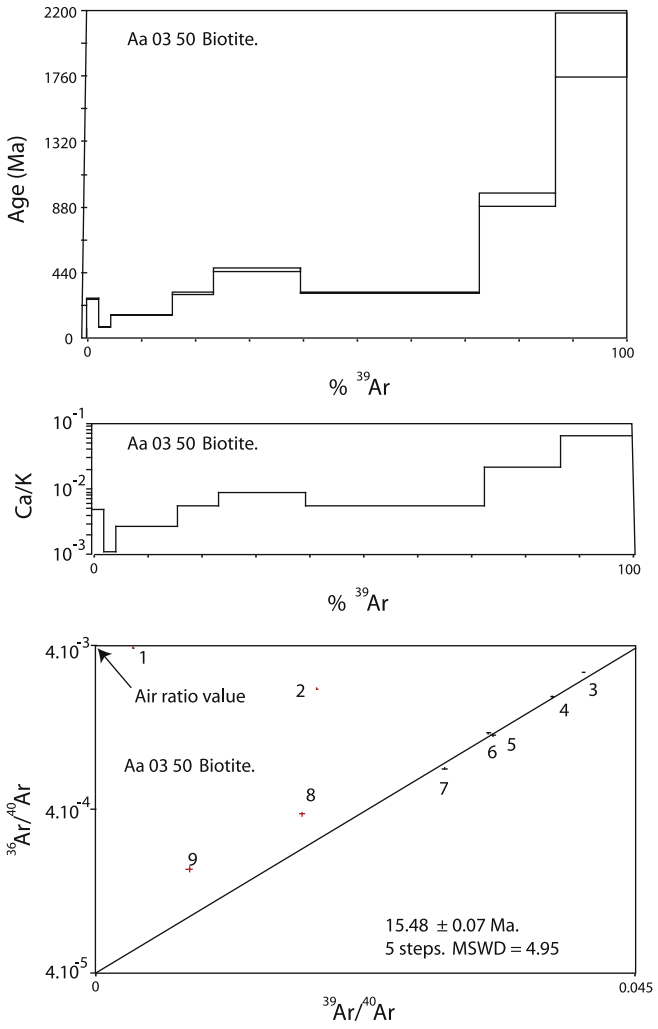

Fig. 9. $^{40}Ar/^{39}Ar$ spectra, Ca/K and isochron correlation diagrams of biotite-rich cataclasite sample Aa0350. Note the excess ^{40}Ar component, especially in the higher temperature steps. The inverse isochron shows mixing of radiogenic argon in the mineral with non-atmospheric argon (initial ratio is far from the expected air value). Thus this shows that the mineral interacted with fluids driving argon from a deep source. As shown in numerous studies (e.g. Leloup et al., 2005; Challandes et al., 2008; Rolland et al., 2008 and references therein) dating of biotite in Alpine shear zones generally shows some excess Ar, while the dating of Hercynian crystals shows disrupted patterns featured by Ar loss. Thus, it is likely that fluids percolating through shear zones were enriched in Ar and that the biotite cataclasite was buffered by these fluids. The sample location is indicated in Fig. 2 and Table 2.

(1) Firstly, the identical phengite and biotite ages from Stage 1 shear zones, as well as the difference between these ages and the consistently younger phengite ages from Stage 2 shear zones, support the conclusion that the Ar–Ar ages reported here represent crystallisation ages and not cooling ages.

(2) The timing of deformation deduced from field observation and Ar dating indicates a multi-stage deformation history. In previous works (e.g. Choukroune and Gapais, 1983; Fourcade et al., 1989; Steck et al., 1989), a general often implicit interpretation was that deformation was progressive in time and space throughout the Aar Massif. The unequivocal geochronological results obtained in this study demonstrate that several deformation stages have occurred, and these are characterized by structural styles evolving from early penetrative foliation development and formation of associated biotite-bearing shear zones, later very localised, phengite-bearing shear zones, then subsequent brittle shear zones. The lack of well-defined plateaus for phengites and biotites in the work of Challandes et al. (2008) may be due to partial resetting or recrystallisation of phengite during subsequent Stage 2 shearing. Challandes et al. also reported Rb–Sr ages of 10–12 Ma for the same samples. They interpreted these results in terms of later re-equilibration of the Rb–Sr system due to fluid percolation through the shear zone network after the cessation of ductile deformation. However, the $^{40}Ar/^{39}Ar$ ages on syn-kinematic phengite obtained in our study are in the same range as the Rb–Sr ages of Challandes et al. This suggests that shear zone formation in the Aar Massif did not cease at 17 Ma. Instead, Stage 1 shear zones were overprinted by subsequent, more localised development of Stage 2 mixed brittle–ductile shear zones at 12–13 Ma. Depending on the intensity of Stage 2 overprinting of Stage 1 shear zones, recrystallisation and fluid circulation related to Stage 2 could explain the partial resetting of both the K–Ar and Rb–Sr systems in Stage 1 shear zones. Our interpretation of the results of Challandes et al. (2008) is that the Rb–Sr system in Stage 1 shear zones was more completely reset than the K–Ar system in phengites. Accordingly, the Rb–Sr isochron of Challandes et al. (2008) shows a good fit, whereas the $^{40}Ar/^{39}Ar$ ages patterns of phengites in Stage 1 shear zones are disrupted due to partial resetting ascribed largely to Stage 2 brittle reactivation and subsequent fluid–rock interaction.

(3) The geodynamic significance of the Stage 2 shear zone development has to be considered at a larger Alpine scale. Ages of Alpine micas obtained in the Helvetic Nappes are mostly between 35 and 20 Ma for a first group of micas associated with the oldest, top-to-north, basal thrusts to the Nappes (Kirschner et al., 2003). A second group of micas giving ages around 15–20 Ma is found mostly adjacent to the Rhone Valley and was interpreted as due to late reactivation, or in response to ongoing Nappe movement. In the light of the structural data obtained in this paper and of recently published work from other External Crystalline Massifs of the Alps (Mont Blanc Massif, Leloup et al., 2005; Rolland et al., 2007, 2008), it appears that this Stage 2 deformation event is strongly transpressive, and that shear zones cross-cut the Nappe pile formerly emplaced between 35 and 20 Ma (Steck, 1984; Burkhard, 1988, 1990; Mancktelow, 1992; Steck and Hunziker, 1994). Therefore, we argue that it corresponds to a change in kinematics within the chain, the Stage 2 shear zone network being formed along the boundary between External and Internal Alps, across the Rhone Valley (e.g. Hubbard and Mancktelow, 1992), possibly in response to the anticlockwise rotation of Apulia (Dewey et al., 1989; Gratier, 1989; Vialon et al., 1989; Mancktelow, 1992). As the Si content in our Stage 2 analysed phengites is found to be similar to those of Stage 1 phengites dated by Challandes et al. (2008), it is suggested that there has been little if any exhumation between Stage 1 and Stage 2 shearing. Using the modelled PT paths computed by Challandes et al. (2008), estimated maximum burial conditions of 0.6 GPa (~20 km) were achieved at 450 °C. We therefore infer that such conditions prevailed during the activity of Stage 2 shear zones at 12–13 Ma. Such conditions are similar to estimates obtained in shear zones formed in the Mont Blanc massif at 15.8–16 Ma (Rolland et al., 2003). The most likely interpretation for the difference in structural style observed between Stage 1 and Stage 2 is that the more progressive character of Stage 1 may be ascribed to their prograde nature in a context of underthrusting during

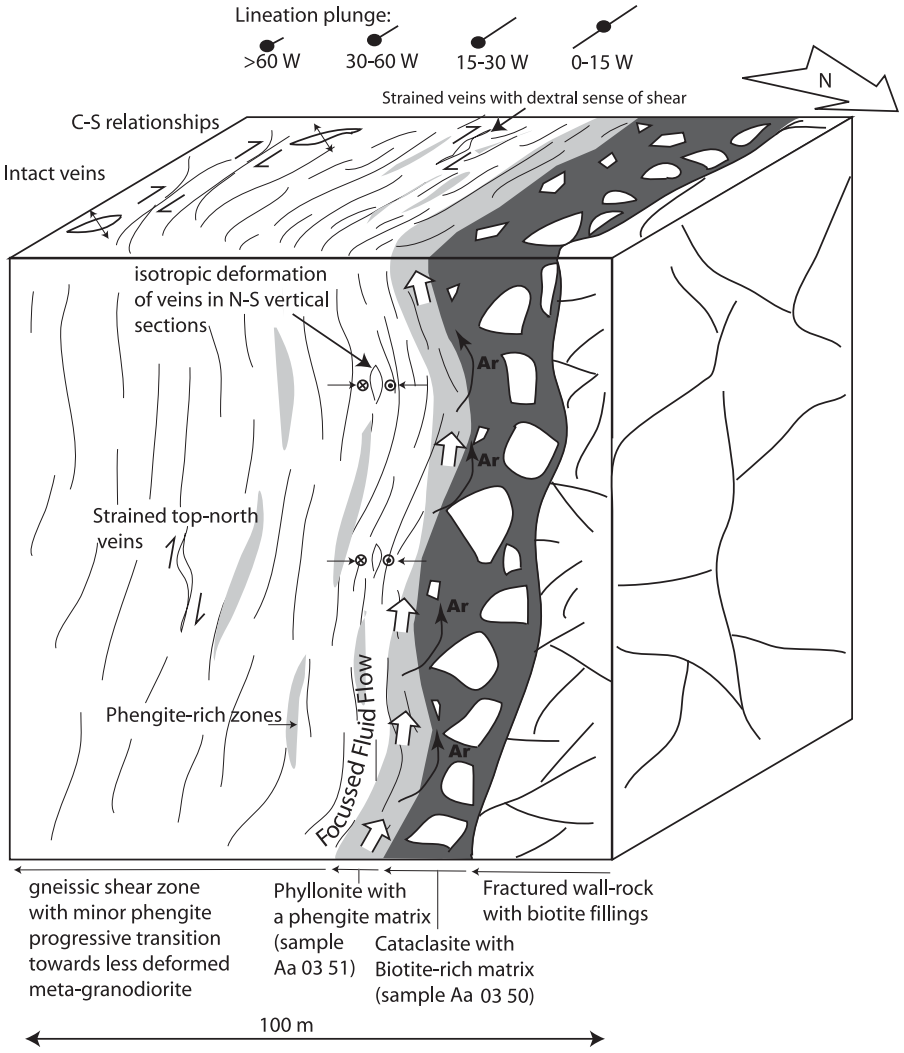

Fig. 10. Sketch of structural relationships in the main Stage 2 shear zone. On the northern side, a biotite-bearing cataclasite is exposed, with a sharp transition to phyllonitic mylonite toward the south. The progressive change in mineral lineation plunge is indicated at the top of the sketch. Also shown is the interpreted fluid pathway, explaining the excess Ar found in the biotite cataclasite.

the progression of collision, while Stage 2 is related to the onset of transpressive tectonics along the Alpine arc. In this view, the Stage 2 shear zones are tied up to the initial stages of exhumation. This change from Stage 1 to Stage 2 is marked by a change in shortening direction from perpendicular to oblique to the belt, and may be related to initiation of Apulian rotation (Collombet et al., 2002). Further, if the two Shear zone stages were formed at relatively similar PT conditions, the extent of fluid–rock interaction must be very different. While Fourcade et al. (1989) and Marquer and Burkhard (1992) interpreted a relatively closed-system for the progressive Stage 1 shear zones, more open-system circulations are likely in Stage 2.

(4) Finally, brittle sinistral Stage 3 faults offset, whereas dextral Stage 3 shear zones reactivate, the Stage 2 shear zones. Within these faults, fluid–rock interaction and neo-crystallisation of clays have also led to isotopic resetting. K–Ar dates of fault gouge clays gave results in the range 9–5 Ma (Kralik et al., 1992), which is significantly younger than our $^{40}Ar/^{39}Ar$ ages on Stage 2 shear zones. These strictly brittle clay-bearing Stage 3 faults establish that at this time the Aar Massif was at conditions below the brittle–ductile transition for quartz (ca. 280–300 °C), indicating relatively rapid exhumation and cooling of the massif from ca. 13 to 9 Ma. Such rapid exhumation is in accordance with exhumation rates estimated from fission track dating since 10 Ma, with an interpreted acceleration in exhumation rates at approximately 5 Ma (see Vernon et al., 2008 for a compilation of results). If a temperature of 300 °C was reached at ~7 Ma, the cooling rate from Stage 2 to Stage 3 would be ~30 °C Ma^{-1}. For an assumed geothermal gradient of 25 °C km^{-1} (e.g. Vernon et al., 2008), this would correspond to an exhumation rate of 1.2 mm a^{-1} and a corresponding exhumation between 12 and 7 Ma from ~20 km to ~14 km depth. The estimated exhumation rate of 1.2 mm a^{-1} is similar to average rates of ~1 mm a^{-1} over the last 16 Ma estimated for the Mont Blanc Massif (Seward and Mancktelow, 1994; Rolland et al., 2007). Finally, Hoffmann et al. (2004) have shown that brittle faulting, brecciation, fluid infiltration and vein development continued in the Grimsel Pass area until at least ca. 3 Ma. This youngest period of deformation was inferred to have been associated with topographically driven flow of meteoric fluids in fault zones. Final exhumation from 300 °C and 14 km to the surface in

the last 7 Ma suggests an average exhumation rate of ~ 2 mm a^{-1}, corresponding to an approximate doubling in exhumation rate since the late Miocene, as proposed by Vernon et al. (2008).

7. Conclusions

Detailed mapping of shear zones and $^{40}Ar/^{39}Ar$ dating of syn-kinematic micas have constrained the relative and absolute ages of several deformation stages near the southern margin of the Aar Massif:

(1) Stage 1 deformation ($\sim$20–22 Ma) produced broad, biotite-rich, ductile shear zones, as confirmed in this study by a biotite-plateau age of 21.1 $\pm$ 0.2 Ma;
(2) Stage 2 deformation (13.8–12.2 Ma) produced relatively narrow, phengite-rich, and predominantly ductile shear zones with phengite ages between 12.2 and 13.8 Ma. Early, biotite-rich cataclastic rock at the margin of some Stage 2 shear zones has Ar–Ar biotite ages indicating excess argon and a possible biotite crystallisation age of 15.5 $\pm$ 0.1 Ma.
(3) Stage 3 deformation ($<$10 Ma) produced brittle faults which cross-cut the earlier structures.

The study has shown that the main Stage 2 shear zone network was preceded by brittle deformation, with an isochron date of $\sim$15.5 Ma, but this age is only indicative. The enhanced permeability due to this fracturing led to a period of enhanced fluid flow, which resulted in the incorporation of excess Ar in the biotite. Subsequent syn-kinematic phengite growth within ductile shear zones is bracketed at 13.8–12.2 Ma, which is similar to published Rb–Sr ages from the Grimsel area. These phengites crystallised during a transpressional phase of brittle–ductile shear zone development that post-dates emplacement of the Helvetic Nappes. Finally, published K–Ar ages obtained on Stage 3 fault gouges show that brittle deformation followed as the result of ongoing (but relatively minor) deformation during exhumation and cooling over the period from 9 to 5 Ma.

Acknowledgements

This research was supported partly by Australian Research Council Discovery grant AA100460, and internal support from Géosciences Azur. The authors warmly thank N. Mancktelow and G. Pennacchioni for their support in the field and thorough discussions on the paper, including correction of the English language, and A.M. Boullier for her encouragements in this study.

Appendix. Supplementary data

Supplementary data associated with this article can be found, in the online version, at doi:10.1016/j.jsg.2009.08.003.

References

Albrecht, J., 1994. Geologic units of the Aar Massif and pre-Alpine rock associations: a critical review. The pre-Alpine crustal evolution of the Aar, Gotthard and Tavetsch massifs. Schweizerische Mineralogische und Petrographische Mitteilungen 74, 5–27.
Arnaud, N.O., Kelley, S.P., 1995. Evidence for excess argon during high pressure metamorphism in the Dora Maira Massif (Western Alps, Italy), using an ultraviolet laser ablation microprobe ^{40}Ar–^{39}Ar technique. Contributions to Mineralogy and Petrology 121, 1–11.
Ayrton, N., Ramsay, J., 1974. Tectonic and metamorphic events in the Alps. Schweizerische Mineralogische und Petrographische Mitteilungen 54, 609–639.
Baxter, E.F., DePaolo, D.J., Renne, P.R., 2002. Spatially correlated anomalous $^{40}Ar/^{39}Ar$ "age" variations in biotites about a lithologic contact near Simplon Pass, Switzerland: a mechanistic explanation for excess Ar. Geochimica et Cosmochimica Acta 66, 1067–1083.
Bertnoat, W., Bambauer, H.U., 1982. The microcline/sanidine transformation isograd in metamorphic regions: II, the region of Lepontine metamorphism, Central Swiss Alps. Schweizerische Mineralogische und Petrographische Mitteilungen 62, 231–244.
Boundy, T.M., Hall, C.M., Li, G., Essene, E.J., Halliday, A.N., 1997. Fine-scale isotopic heterogeneities and fluids in the deep crust: a $^{40}Ar/^{39}Ar$ laser ablation and TEM study of muscovites from a granulite–eclogite transition zone. Earth and Planetary Science Letters 148, 223–242.
Burkhard, M., 1988. ÍHélvetique de la bordure occidentale du massif de ÍAar (évolution tectonique et métamorphique). Eclogae Geologicae Helvetiae 81, 63–114.
Burkhard, M., 1990. Aspects of the large-scale Miocene deformation in the most external part of the Swiss Alps (Subalpine molasse to Jura fold belt). Eclogae Geologicae Helvetiae 83, 559–583.
Bussy, F., von Raumer, J.F., 1994. U–Pb geochronology of Palaeozoic magmatic events in the Mont Blanc crystalline massif, Western Alps. Schweizerische Mineralogische und Petrographische Mitteilungen 74, 514–515.
Challandes, N., 2001. Comportement des systèmes isotopiques $^{40}Ar/^{39}Ar$ et Rb-Sr dans les zones de cisaillement: Exemples du massif de l'Aar (Massifs Cristallins Externes) et de la nappe de Suretta (Alpes Centrales Suisses). Ph. D. University of Neuchatel, Switzerland.
Challandes, N., Marquer, D., Villa, I.M., 2003. Dating the evolution of C–S microstructures: a combined $^{40}Ar/^{39}Ar$ step-heating and UV laserprobe analysis of the Alpine Roffna shear zone. Chemical Geology 197, 3–19.
Challandes, N., Marquer, D., Villa, I.M., 2008. P-T-t modelling, fluid circulation, and ^{39}Ar–^{40}Ar and Rb–Sr mica ages in the Aar Massif shear zones (Swiss Alps). Swiss Journal of Geosciences 101, 269–288.
Choukroune, P., Gapais, D., 1983. Strain pattern in the Aar granite (Central Alps); orthogneiss developed by bulk inhomogeneous flattening. Journal of Structural Geology 5, 411–418.
Collombet, M., Thomas, J.C., Chauvin, A., Tricart, P., Bouillin, J.P., Gratier, J.P., 2002. Counterclockwise rotation of the western Alps since the Oligocene: new insights from paleomagnetic data. Tectonics 21, 1032. doi:10.1029/2001TC901016.
Cox, S.F., Etheridge, M.A., Wall, V.J., 1987. The role of fluids in syntectonic mass transport, and localization of metamorphic vein-type ore deposits. Ore Geology Reviews 2, 65–86.
Cumbest, R.J., Johnson, E.L., Onstott, T.C., 1994. Argon composition of metamorphic fluids: implications for $^{40}Ar/^{39}Ar$ geochronology. Geological Society of America Bulletin 106, 942–951.
DeJong, K., Féraud, G., Ruffet, G., Amouric, M., Wijbrans, J.R., 2001. Excess argon incorporations in phengite of the Mulhacen complex: submicroscopic illitization and fluid ingress during late Miocene extension in the Betic zone, southeastern Spain. Chemical Geology 178, 159–195.
Dempster, T.J., 1986. Isotope systematics in minerals: biotite rejuvenation and exchange during Alpine metamorphism. Earth and Planetary Science Letters 78, 355–367.
Dewey, J.F., Helman, M.L., Turco, E., Hutton, D.H.W., Knott, S.D., 1989. Kinematics of the western Mediterranean. In: Coward, M.P., Dietrich, D., Park, R.G. (Eds.), Alpine Tectonics. Geological Society of London, Special Publications, vol. 45, pp. 265–283.
Dodson, M.H., 1973. Closure temperature in cooling geochronological and petrological systems. Contributions to Mineralogy and Petrology 40, 259–274.
Dunlap, W.J., 1997. Neocrystallization or cooling? $^{40}Ar/^{39}Ar$ ages of white micas from low-grade mylonites. Chemical Geology 143, 181–203.
Dunlap, W.J., Kronenberg, A.K., 2001. Argon loss during deformation of micas: constraints from laboratory deformation experiments. Contributions to Mineralogy and Petrology 141, 174–185.
Foland, K.A., 1979. Limited mobility of argon in a Metamorphic Terrain. Geochim. Cosmochim. Acta 43, 793–801.
Foland, K.A., 1983. $^{40}Ar/^{39}Ar$ incremental heating plateaus for biotites with excess argon. Isotope Geoscience 1, 3–21.
Fourcade, S., Marquer, D., Javoy, M., 1989. $^{18}O/^{16}O$ variations and fluid circulation in a deep shear zone: the case of the alpine ultramylonites from the Aar massif (Central Alps, Switzerland). Chemical Geology 77, 119–131.
Frey, M., 1987. Low Temperature Metamorphism. Chapman and Hall, New York, 351 pp.
Frey, M., 1988. Discontinuous inverse metamorphic zonation, Glarus Alps, Switzerland: evidence from illite "crystallinity"'data. Schweizerische Mineralogische und Petrographische Mitteilungen 68, 171–183.
Frey, M., Desmons, J., Neubauer, F., 1999. The new metamorphic map of the Alps: introduction. Schweizerische Mineralogische und Petrographische Mitteilungen 79, 1–4.
Frey, M., Mählmann Ferreiro, R., 1999. Alpine metamorphism of the Central Alps (Central Alps, Alpine metamorphism, low-grade metamorphism, P-T-t path). Schweizerische Mineralogische und Petrographische Mitteilungen 79, 135–154.
Frey, M., Teichmüller, M., Teichmüller, R., Mullis, J., Künzi, B., Breitschmid, A., Gruner, U., Schwier, B., 1980. Very low-grade metamorphism in external parts of the Central Alps: illite crystallinity, coal rank and fluid inclusion data. Eclogae Geologicae Helvetiae 73, 173–203.
Goodwin, L.B., Renne, P.R., 1991. Effects of progressive mylonitization on Ar retention in biotites from the Santa Rosa mylonite zone (California), and thermochronologic implications. Contributions to Mineralogy and Petrology 108, 283–297.

Gratier, J.-P., 1989. Strain–displacement compatibility and restoration of the Chaînes Subalpines of the Western Alps. In: Coward, M.P., Dietrich, D., Park, R.G. (Eds.), Alpine Tectonics. Geological Society of London, Special Publications, vol. 45, pp. 65–81.

Guermani, A., Pennacchioni, G., 1998. Brittle precursors of plastic deformation in a granite: an example from the Mont Blanc massif (Helvetic, western Alps). Journal of Structural Geology 20, 135–148.

Hames, W.E., Bowring, S.A., 1994. An empirical evaluation of the argon diffusion geometry in muscovite. Earth and Planetary Science Letters 124, 161–167.

Harrison, T.M., Armstrong, R.L., Naeser, C.W., Harakal, J.E., 1979. Geochronology and thermal history of the Coast Plutonic complex, near Prince Rupert BC. Canadian Journal of Earth Sciences 16, 400–410.

Harrison, T.M., McDougall, I., 1981. Excess ^{40}Ar in metamorphic rocks from Broken Hill, New South Wales: implications of ^{40}Ar/^{39}Ar age spectra and the thermal history of the region. Earth and Planetary Science Letters 55, 123–149.

Hoffmann, B.A., Helfer, M., Diamond, L.W., Villa, I.M., Frei, R., Eikenberg, J., 2004. Topography-driven hydrothermal breccia mineralization of Pliocene age at Grimsel Pass, Aar massif, Central Swiss Alps. Schweizerische Mineralogische und Petrographische Mitteilungen 84, 271–302.

Hubbard, M., Mancktelow, N.S., 1992. Lateral displacement during Neogene convergence in the western and central Alps. Geology 20, 943–946.

Huber, M., Ramsay, J., Simpson, C., 1980. Deformation in the Maggia and Antigorio nappes, Lepontine Alps. Eclogae Geologicae Helvetiae 73, 593–606.

Jourdan, F., Féraud, G., Bertrand, H., Kampunzu, A.B., Tshoso, G., Le Gall, B., Tiercelin, J.J., Capiez, P., 2004. The Karoo triple junction questioned: evidence for Jurassic and Proterozoic ^{40}Ar/^{39}Ar ages and geochemistry of the giant Okavango dyke swarn (Botswana). Earth and Planetary Science Letters 222, 989–1006.

Kelley, S.P., 1988. The relationship between K–Ar mineral ages, mica grain sizes and movement on the Moine Thrust Zone, NW Highlands, Scotland. Journal of the Geological Society, London 145, 1–10.

Kelley, S.P., 2002. Excess argon in K–Ar and Ar–Ar geochronology. Chemical Geology 188, 1–22.

Kelley, S.P., Arnaud, N.O., Turner, S.P., 1994. High-spatial resolution ^{40}Ar/^{39}Ar investigations using an ultra-violet laser probe extraction technique. Geochimica et Cosmochimica Acta 58, 3519–3525.

Kerrich, R., 1986. Fluid infiltration into fault zones: chemical, isotopic, and mechanical effects. Pure and Applied Geophysics 124, 225–268.

Kirschner, D.L., Cosca, M.A., Masson, H., Hunziker, J.C., 1996. Staircase ^{40}Ar/^{39}Ar spectra of fine-grained white mica; timing and duration of deformation and empirical constraints on argon diffusion. Geology 24, 747–750.

Kirschner, D.L., Masson, H., Sharp, Z.D., 1999. Fluid migration through thrust faults in the Helvetic Nappes (Western Swiss Alps). Contributions to Mineralogy and Petrology 136, 169–183.

Kirschner, D.L., Masson, H., Cosca, M.A., 2003. An ^{40}Ar/^{39}Ar, Rb/Sr, and stable isotope study of micas in low-grade fold-and-thrust belt: an example from the Swiss Helvetic Alps. Contributions to Mineralogy and Petrology 145, 460–480.

Kligfield, R., Hunziker, J., Dallmeyer, R.D., Schamel, S., 1986. Dating deformation phases using K–Ar and ^{40}Ar/^{39}Ar techniques: results from the Northern Apennines. Journal of Structural Geology 8, 781–798.

Kralik, M., Clauer, N., Holnsteiner, R., Huemer, H., Kappel, F., 1992. Recurrent fault activity in the Grimsel test site (GTS, Switzerland), revealed by Rb–Sr, K–Ar and tritium isotope techniques. Journal of the Geological Society, London 149, 293–301.

Kramar, N., Cosca, M.A., Hunziker, J.C., 2001. Heterogeneous ^{40}Ar* distributions in naturally deformed muscovite: in-situ UV-laser ablation evidence for microstructurally controlled diffusion. Earth and Planetary Science Letters 192, 377–388.

Labhart, T.P., 1977. Aarmassiv und Gotthardmassiv. Sammlung geologischer Führer. Gebrüder Borntraeger, Berlin, Stuttgart, 173 pp.

Leloup, P.H., Arnaud, N., Sobel, E.R., Lacassin, R., 2005. Alpine thermal and structural evolution of the highest external crystalline massif: the Mont Blanc. Tectonics 24, TC4002. doi:10.1029/2004TC001676.

Lo, C.H., Onstott, T.C., 1989. ^{39}Ar recoil artifacts in chloritized biotite. Geochimica et Cosmochimica Acta 53, 2697–2711.

Lovering, J.F., Richards, J.R., 1964. Potassium–argon age study of possible lower crust and upper-mantle inclusions in deep-seated intrusions. Journal of Geophysical Research 69, 4895–4901.

Mancktelow, N.S., 1992. Neogene lateral extension during convergence in the Central Alps: evidence from interrelated faulting and backfolding around the Simplonpass (Switzerland). Tectonophysics 215, 295–317.

Mancktelow, N.S., Pennacchioni, G., 2005. The control of precursor brittle fracture and fluid–rock interaction on the development of single and paired ductile shear zones. Journal of Structural Geology 27, 645–661.

Marquer, D., 1987. Transfert de matière et déformation progressive des granitoïdes; exemples des massifs de l'Aar et du Gotthard. Thèse, Université de Rennes, 288 p.

Marquer, D., 1989. Transferts de matières et déformation des granitoïdes. Aspects méthodologiques. Schweizerische Mineralogische und Petrographische Mitteilungen 69, 13–33.

Marquer, D., Burkhard, M., 1992. Fluid circulation, progressive deformation and mass-transfer processes in the upper crust: the example of basement–cover relationships in the External Crystalline Massifs, Switzerland. Journal of Structural Geology 14, 1047–1057.

Marquer, D., Gapais, D., 1985. Les massifs cristallins externes sur une transversale Guttanen-Val Bedretto (Alpes centrales): structures et histoire cinématique. Comptes rendus de l'Académie des sciences. Série 2, Mécanique, Physique, Chimie, Sciences de l'univers, Sciences de la Terre 301, 543–546.

Marquer, D., Gapais, D., Capdevila, R., 1985. Comportement chimique et orthogneissification d'une granodiorite en faciès schistes verts (Massif de l'Aar, Alpes centrales suisses). Bulletin de Minéralogie 108, 209–221.

Marquer, D., Peucat, J.J., 1994. Rb–Sr systematics of recrystallized shear zones at the greenschist–amphibolite transition: examples from granites in the Swiss Central Alps. Schweizerische Mineralogische und Petrographische Mitteilungen 74, 343–358.

McCaig, A.M., Wickham, S.M., Taylor, H.P., 1990. Deep fluid circulation in Alpine shear zones, Pyrenees, France: field and oxygen isotope studies. Contributions to Mineralogy and Petrology 106, 41–60.

McDougall, I., Harrison, M.T., 1999. Geochronology and Thermochronology by the ^{40}Ar/^{39}Ar Method, second ed. Oxford University Press.

Michalski, I., Soom, M., 1990. The Alpine thermo-tectonic evolution of the Aar and Gotthard massifs, Central Switzerland: fission track ages on zircon and apatite and K–Ar mica ages. Schweizerische Mineralogische und Petrographische Mitteilungen 70, 373–387.

Milnes, A.G., 1974. Post-nappe folding in the western Lepontine Alps. Eclogae Geologicae Helvetiae 67, 333–348.

Mulch, A., Cosca, M.A., Handy, M.R., 2002. In-situ UV-laser ^{40}Ar/^{39}Ar geochronology of a micaceous mylonite: an example of defect-enhanced argon loss. Contributions to Mineralogy and Petrology 142, 738–752.

Müller, W., Aerden, D., Halliday, A.N., 2000a. Isotopic dating of strain fringe increments: duration and rates of deformation in shear zones. Science 288, 2195–2198.

Müller, W., Mancktelow, N.S., Meier, M., 2000b. Rb–Sr microchrons of synkinematic mica in mylonites: an example from the DAV fault of the Eastern Alps. Earth and Planetary Science Letters 180, 385–397.

O'Hara, K., 1988. Fluid flow and volume loss during mylonitization: an origin for phyllonite in an overthrust setting, North Carolina, USA. Tectonophysics 156, 21–36.

Pennacchioni, G., 2005. Control of the geometry of precursor brittle structures on the type of ductile shear zone in the Adamello tonalites, Southern Alps (Italy). Journal of Structural Geology 27, 627–644.

Pennacchioni, G., Mancktelow, N.S., 2007. Nucleation and initial growth of a shear zone network within compositionally and structurally heterogeneous granitoids under amphibolite facies conditions. Journal of Structural Geology 29, 1757–1780.

Pfiffner, O.A., Frei, W., Valasek, P., Sfauble, M., Levato, L., DuBois, L., Schmid, S.M., Smithson, S.B., 1990. Crustal shortening in the Alpine orogen: results from deep seismic reflection profiling in the eastern Swiss Alps, Line NFP20-EAST. Tectonics 9, 1327–1355.

Purdy, J.W., Jäger, E., 1976. K–Ar ages on rock-forming minerals from the Central Alps. Memorie degli Istituti di Geologia e Mineralogia dell'Università di Padova 30, 1–28.

Reddy, S.M., Kelley, S.P., Wheeler, J., 1996. A ^{40}Ar/^{39}Ar laser probe study of micas from the Sesia Zone, Italian Alps: implications for metamorphic and deformation histories. Journal of Metamorphic Geology 14, 493–508.

Roddick, J.C., Cliff, R.A., Rex, D.C., 1980. The evolution of excess argon in alpine biotites – a ^{40}Ar–^{39}Ar analysis. Earth and Planetary Science Letters 48, 185–208.

Rolland, Y., Cox, S.F., Boullier, A.M., Pennacchioni, G., Mancktelow, N., 2003. Rare Earth and trace element mobility and fractionation in mid-crustal shear zones: insights from the Mont-Blanc Massif (Western Alps). Earth and Planetary Science Letters 214, 203–219.

Rolland, Y., Corsini, M., Rossi, M., Cox, S.F., Pennacchioni, G., Mancktelow, N., Boullier, A.M., 2007. Comment on "Alpine thermal and structural evolution of the highest external crystalline massif: The Mont Blanc" by P.H. Leloup, N. Arnaud, E.R. Sobel, and R. Lacassin. Tectonics 26, TC2015. doi:10.1029/2006TC001956.

Rolland, Y., Rossi, M., Cox, S.F., Corsini, M., Boullier, A.M., Pennachioni, G., Mancktelow, N., 2008. ^{40}Ar/^{39}Ar dating of syn-kinematic white mica: insights for fluid–rock reaction in low-grade shear zones (Mont Blanc Massif) and constraints on timing of deformation in the NW external Alps. In: Wibberley, C., Kurtz, W., Imber, J., Holdsworth, R.E., Collettini, C. (Eds.), The Internal Structure of Fault Zones: Implications for Mechanical and Fluid-Flow Properties. Geological Society of London, Special Publications, pp. 293–315. doi:10.1144/SP299.17.

Scaillet, S., 1996. Excess ^{40}Ar transport scale and mechanism in high-pressure phengites; a case study from an eclogitized metabasite of the Dora-Maira nappe, Western Alps. Geochimica et Cosmochimica Acta 60, 1075–1090.

Schaltegger, U., 1994. Unravelling the pre-Mesozoic history of Aar and Gotthard massifs (central Alps) by isotopic dating: a review. Schweizerische Mineralogische und Petrographische Mitteilungen 74, 41–51.

Segall, P., Simpson, C., 1986. Nucleation of ductile shear zones on dilatant fractures. Geology 14, 56–59.

Seward, D., Mancktelow, N.S., 1994. Neogene kinematics of the central and western Alps: evidence from fission-track data. Geology 22, 803–806.

Sherlock, S., Kelley, S.P., Zalasiewicz, J.A., Schofield, D.I., Evans, J.A., Merriman, R.J., Kemp, S.J., 2003. Precise dating of low-temperature deformation: Strain-fringe analysis by ^{40}Ar–^{39}Ar laser microprobe. Geology 31, 219–222.

Simon-Labric, T., Rolland, Y., Dumont, T., Heymes, T., Authemayou, C., Corsini, M., Fornari, M., 2009. ^{40}Ar/^{39}Ar dating of Penninic Front tectonic displacement (W Alps) during the Lower Oligocene (31–34 Ma). Terra Nova 21, 127–136.

Soom, M.A., 1990. Abkuhlungs- und Hebungsgeschichte der Externmassive und der Penninischen Decken beidseits der Simplon-Rhone-Linie seit dem Oligozen: Spaltspurdatierungen an Apatit/Zirkon und K–Ar-Datierungen an Biotit/Muskowit (westliche Zentralalpen). Thesis. University of Bern, Bern, Switzerland, 119 pp.

Steck, A., 1966. Petrographische und tektonische Untersuchungen am zentralen Aaregranit und seinen altkristallinen Huellgesteinen im westlichen Aarmassiv im Gebiet belalp-Grisighorn. Beiträge zur geologischen Karte der Schweiz 130, 96.

Steck, A., 1968. Die alpinischen strukturen in den zentralen Aargraniten des westlichen Aarmassivs. Eclogae Geologicae Helvetiae 61, 19–48.

Steck, A., 1976. Albit-Oligoklas-Mineralgesellschaften der Peristeritluecke aus alpinmetamorphen Granitgneisen des Gotthardmassivs. Schweizerische Mineralogische und Petrographische Mitteilungen 56, 269–292.

Steck, A., 1984. Structures de déformation tertiaires dans les Alpes centrales (transversale Aar-Simplon-Ossola). Eclogae Geologicae Helvetiae 77, 55–100.

Steck, A., Bigioggero, B., Dal Piaz, G.V., Escher, A., Martinotti, G., Masson, H., 1999. Carte tectonique des Alpes de Suisse occidentale et des régions avoisinantes 1:100,000. In: Carte géologique spéciale No 123. Swiss National Hydrological and Geological Survey, CH-3003 Berne, Switzerland.

Steck, A., Burri, G., 1971. Chemismus und Paragenesen von Granaten aus Granitgneisen der Grünschiefer- und Amphibolitfazies der Zentralalpen. Schweizerische Mineralogische und Petrographische Mitteilungen 51, 534–538.

Steck, A., Epard, J.L., Escher, A., Marchand, R., Masson, H., Spring, L., 1989. Coupe tectonique horizontale des Alpes centrales. In: Mémoires de Géologie Lausanne 5, 8 pp.

Steck, A., Hunziker, J., 1994. The Tertiary structural and thermal evolution of the Central Alps: compressional and extensional structures in an orogenic belt. Tectonophysics 238, 229–254.

Steiger, R.H., Jäger, E., 1977. Subcomission on geochronology: convention of the use of decay constants in geo- and cosmochronology. Earth and Planetary Science Letters 36, 359–362.

Tikoff, B., Teyssier, C., 1994. Strain modelling of displacement–field partitioning in transpressional orogens. Journal of Structural Geology 16, 1575–1588.

Turner, G., Huneke, J.C., Podose, F.A., Wasserburg, G.J., 1971. $^{40}Ar/^{39}Ar$ ages and cosmic ray exposure ages of Apollo 14 samples. Earth and Planetary Science Letters 12, 15–19.

Vernon, A.J., van der Beek, P.A., Sinclair, H.D., Rahn, M.K., 2008. Increase in late Neogene denudation of the European Alps confirmed by analysis of a fission-track thermochronology database. Earth and Planetary Science Letters 270, 316–329.

Vialon, P., Rochette, P., Ménard, G., 1989. Indentation and rotation in the western Alpine arc. In: Coward, M.P., Dietrich, D., Park, R.G. (Eds.), Alpine Tectonics. Geological Society of London, Special Publications, vol. 5, pp. 329–338.

Villa, I.M., 1998. Isotopic closure. Terra Nova 10, 42–47.

Villa, I.M., Ruggieri, G., Puxeddu, M., 1997. Petrological and geochronological discrimination of two white-mica generations in a granite cored from the Larderello-Travale geothermal field (Italy). European Journal of Mineralogy 9, 563–568.

von Raumer, J.F., 1984. The External Massifs, relics of Variscan basement in the Alps. Geologische Rundschau 73, 1–31.

von Raumer, J.F., Abrecht, J., Bussy, F., Lombardo, B., Ménot, R.P., Schaltegger, U., 1999. The Palaeozoic metamorphic evolution of the Alpine External Massifs. Schweizerische Mineralogische und Petrographische Mitteilungen 79, 5–22.

Wagner, G.A., Reimer, G.M., Jäger, E., 1977. Cooling ages derived by apatite fission-track, mica Rb–Sr and K–Ar dating: the uplift and cooling history of the Central Alps. Memorie degli Istituti di Geologia e Mineralogia dell'Università di Padova 30, 1–28.

West, D.P., Lux, D.R., 1993. Dating mylonitic deformation by the ^{40}Ar–^{39}Ar method: an example from the Norumbega Fault Zone, Maine. Earth and Planetary Science Letters 120, 221–237.

Wijbrans, J.R., McDougall, I., 1986. $^{40}Ar/^{39}Ar$ dating of white micas from an Alpine high-pressure metamorphic belt on Naxos (Greece) – the resetting of the argon isotopic system. Contributions to Mineralogy and Petrology 93, 187–194.